Mechanisms underlying the hyperexcitability of CA3 and dentate gyrus hippocampal neurons derived from bipolar disorder patients.

Shani Stern, Anindita Sarkar, Tchelet Stern, Arianna Mei, Ana P.D. Mendes, Yam Stern, Gabriela Goldberg, Dekel Galor, Thao Nguyen, Lynne Randolph-Moore, et al.

Mechanisms underlying the hyperexcitability of CA3 and dentate gyrus hippocampal neurons derived from bipolar disorder patients.

Shani Stern[1], Anindita Sarkar[1], Arianna Mei[1], Tchelet Stern[1], Ana P. D. Mendes[1], Yam Stern[1], Gabriela Goldberg[1], Thao Nguyen[1], Lynne Randolph-Moore[1], Yongsung Kim[1], Guy Rouleau[2], Anne Bang[3], Martin Alda[4], Renata Santos[5], Maria C. Marchetto[1], Fred H. Gage[1]

1 Laboratory of Genetics, Gage, Salk Institute for Biological Studies, 10010 North Torrey Pines Road, La Jolla, CA 92037, USA

2 Montreal Neurological Institute, McGill University, Montreal

3 Conrad Prebys Center for Chemical Genomics, Sanford Burnham Prebys Medical Discovery Institute, 10901 North Torrey Pines Road, La Jolla, CA 92037, USA

4 Department of Psychiatry, Dalhousie University, 5909 Veterans' Memorial Lane, Halifax, NS, B3H 2E2, Canada

5 Laboratory of Dynamic of Neuronal Structure in Health and Disease, Institute of Psychiatry and Neuroscience of Paris (UMR_S1266 INSERM, University Paris Descartes), 102 rue de la Santé, 75014 Paris, France

Corresponding author: Fred H. Gage, gage@salk.edu

Abstract

Approximately one in every 50 people is affected with bipolar disorder (BD), making this disease a major economic burden. Having previously studied the phenotype of dentate gyrus granule neurons derived from BD patients, we turned our attention to studying the phenotype of CA3 pyramidal neurons. We found that CA3 BD neurons were hyperexcitable only when derived from patients who responded to lithium. The higher amplitudes and faster kinetics of fast potassium currents correlated with this hyperexcitability. Further supporting the involvement of the fast potassium currents in this hyperexcitability and sustained activity, we observed an overexpression of Kcnc1 and Kcnc2 in hippocampal neurons derived from lithium responders. We therefore applied specific fast potassium channel blockers, which diminished the hyperexcitability. When differentiating this cohort into spinal motor neurons, we did not observe any physiological changes between BD motor neurons and control motor neurons, suggesting that the physiological alterations were neuronal type specific in BD.

Introduction

Bipolar disorder (BD) affects around 1-2.5% of the worldwide population, depending on the severity of the symptoms (Grande et al., 2016; Merikangas et al., 2007; Van Meter et al., 2011). People with this disorder suffer from episodes of mania and depression and, without treatment, are at high risk of suicide (Jamison, 2000). This disorder places a major economic burden on the health system. Lithium is still among the first-line treatments for both acute episodes and long-term prevention of manic and depressive recurrences. However, a large proportion of patients do not respond to lithium and they are sometimes treated for long periods before a clinician realizes that they are non-responders. In addition, some patients experience side effects from lithium such as tremor, polyuria or reduced kidney function (Gitlin, 2016).

Like other psychiatric disorders, BD has a complex genetic background; many genes are known to associate with it (Ferreira et al., 2008; Gershon et al., 2011; Muhleisen et al., 2014) but each gene is considered a subtle addition to disease susceptibility, and there are no genes that have a large impact. Some of the known associations include ANK3 and CACNA1C (Ferreira et al., 2008), ODZ4 (Psychiatric, 2011), BDNF (Neves-Pereira et al., 2002), DGKH (Baum et al., 2008) and other risk loci; some are shared with multiple psychiatric disorders (Forstner et al., 2017; Green et al., 2010; Huang et al., 2010). These complex genetics slowed down research into BD before the introduction of induced pluripotent stem cells (iPSCs), since most of that earlier research had to be done in post-mortem tissue. Gene expression differences were found in post-mortem tissue of the frontal cortex in genes such as TGF-β, Casp-8 and Tob (Bezchlibnyk et al., 2001). Decreased levels of the major brain antioxidant, glutathione, were found in the post-mortem prefrontal cortex of patients with BD and other psychiatric disorders (Gawryluk et al., 2011). Distinct proteomic profiles of pituitary glands from post-mortem tissue of BD patients were also reported (Stelzhammer et al., 2015). But generally, experiments using post-mortem tissue were obviously limited. Upon the development of iPSC techniques, the study of this disease took a large step forward, enabling measurements of neurons that were derived directly from BD patients. Moreover, these neurons could be generated from patients with distinct clinical characteristics.

The hyperexcitability phenotype of dentate gyrus (DG) hippocampal neurons derived from BD patients was first reported in our initial study (Mertens et al., 2015) using gene expression profiles, where mitochondrial defects were also detected. We replicated these findings in another cohort, showing again that DG hippocampal neurons were hyperexcitable (Stern et al., 2018). The hyperexcitability in both studies was assessed using the total number of evoked action potentials in a few current steps, which would reflect on the ability of BD DG neurons to sustain activity with a high current injection. In

addition, we found that the physiology of the neurons derived from lithium-responsive (LR) patients was very different than the physiology of neurons derived from non-responsive (NR) patients. Other studies have shown differences in the transcriptomics of neurons derived from BD patients (Kim et al., 2015) and changes in the expression of genes critical for neuroplasticity such as WNT pathway components and ion channel subunits (Madison et al., 2015). Tobe et al. (Tobe et al., 2017) used proteomics profiling of human iPSCs (hiPSCs) from BD patients and showed that lithium changed the phosphorylation of CRMP2. These authors found that the ratio of phosphorylated to unphosphorylated CRMP2 was elevated only in BD patients who responded to lithium. Lithium lowered the ratio and spine density, acting through phosphorylation of CRMP2. Overall, the use of iPSCs has enabled the identification of an endophenotype of hyperexcitability, but generally the mechanisms underlying the causes of BD remain elusive, leaving us still far from finding better treatment. In addition to our general lack of understanding of the mechanisms of this disease, the understanding of the mechanisms by which lithium acts to reduce the number of episodes in BD patients is not complete. Lithium is the most recommended drug today for BD patients, but the majority of patients either do not respond or only partially respond to lithium treatment.

In this study, we used a new protocol that we recently developed (Sarkar et al., 2018) to search for a phenotype in CA3 pyramidal neurons of the hippocampus. We have found a similar phenotype of hyperexcitability (measured similarly as the total evoked potentials in a few current steps), but only in the neurons derived from the LR patients. We delved deeper into the mechanistic causes that produced these hyperexcitable neurons, which have an extraordinary capability of sustained and high frequency activity. We observed that this hyperexcitability was highly correlated with the amplitude and fast kinetics of the fast potassium channels. qPCR confirmed that Kv3.1 and Kv3.2 were over-expressed in these BD LR neurons, further supporting the involvement of fast kinetics potassium channels. BD NR neurons, although not being as significantly hyperexcitable as CA3 neurons compared to the control CA3 neurons, had alterations in their physiological properties such as drastically reduced sodium currents and increased fast potassium currents, but the latter had a slower kinetics than the LR neurons' fast potassium currents. A non-CNS neuron that we measured - the spinal motor neuron - did not show any physiological difference that we could identify between neurons derived from BD patients and control individuals, further showing that the physiological changes are neuronal type specific.

Methods

Patients

The cohort in this study consisted of the same patients used in the previous study (Stern et al., 2018). Supplementary table 1 summarizes their clinical data.

Cell culture: DG neurons

DG granule neurons were cultured according to our published protocol (Yu et al., 2014), and measurements were performed on these neurons approximately 4.5 weeks after the start of the differentiation date, which is about a week later than the measurement in our previous study (Stern et al., 2018). This 4.5-week time point is denoted throughout the manuscript as t2; an earlier time point of around 2.5 weeks is denoted as t1.

Cell culture: CA3 neurons

CA3 pyramidal neurons were cultured according to our published protocol (Sarkar et al., 2018) and measured at t1 or t2.

Cell culture: motor neurons

Motor neurons were cultured according to our published protocol (Marchetto et al., 2008).

RNA preparation and qPCR: CA3 neurons

Total cellular RNA was extracted from 3-5 million cells per sample at 30 days post-differentiation using the RNA-BEE (QIAGEN), according to the instructions supplied with the kit, and reverse transcribed using the high-capacity cDNA synthesis kit from AB Biosystems. qPCR was done using SYBR green (Life Technologies). Samples with cycle threshold (CT) values of more than 30 were discarded from the analysis. qPCR results were analyzed using SDS Software v 3.2 for a 7900HT real-time PCR system.

Whole cell patch clamp

Neurons were infected with the ELAVL2::eGFP lentiviral vector at 15 days differentiation (as previously reported; (Sarkar et al., 2018). Neurons on glass coverslips were transferred to a recording chamber in standard recording medium containing (in mM) 10 HEPES, 4 KCl, 2 CaCl2,1 MgCl2, 139 NaCl, and 10 D-glucose (310 mOsm, pH 7.4). Whole-cell patch-clamp recordings were performed from ELAVL2::eGFP-highlighted CA3 pyramidal neurons [the neurons patched were typically the larger cells in all the groups, which is customary in the field (Stern et al., 2015), with bright ELAVL2::eGFP expression], typically at 2 recording dates: around 2.5 weeks of differentiation (t1) and at 30-35 days of differentiation (t2). Patch electrodes were filled with internal solutions containing (in mM) 130 K-gluconate, 6 KCl, 4 NaCl, 10 Na-HEPES, 0.2 K-EGTA, 0.3 GTP, 2 Mg-ATP, 0.2 cAMP, 10 Dglucose, 0.15% biocytin and 0.06% rhodamine. The pH and osmolarity of the internal solution were brought close to physiological conditions (pH 7.3, 290–300 mOsmol) (pipette tip resistance was typically 10–15MΩ). Signals were amplified with aMulticlamp700B amplifier and recorded with Clampex 10.2 software (Axon Instruments). Data were acquired at a sampling rate of 20 kHz and analyzed using Clampfit-10 and the software package Matlab (2014b, The MathWorks Inc., Natick, MA, 2000). All measurements were conducted at room temperature.

Lithium treatment

Cultures of CA3 neurons were treated with 1 mM LiCl starting at 16 days of differentiation by exchanging 50% of the media daily, similar to the chronic treatment they had been exposed to in our previous study (Stern et al., 2018), Electrophysiological recordings were conducted at 30-35 days of differentiation (t2).

Analysis of electrophysiological recordings

Total evoked action potentials

Similar to our previous study (Stern et al., 2018), cells were typically held in current clamp mode near -60 mV with a steady holding current, and current injections were given starting 5 pA below the steady holding current, in 3 pA steps of 400 ms in duration. A total of 35 depolarization steps were given. Neurons that needed a current injection of more than 50 pA to be held at -60 mV were discarded from the analysis. The total number of action potentials was counted in 35 depolarization steps, starting from the first depolarization step, which was 10 pA below the current and caused the membrane potential to be at -60 mV (typically around 0).

Spike shape analysis

The first evoked action potential was used for spike shape analysis (with the lowest injected current needed for eliciting an action potential). Spike threshold was the membrane potential at which the slope of the depolarizing membrane potential increased drastically, resulting in an action potential (the first maximum in the second derivative of the voltage vs. time). The 5-ms AHP amplitude was calculated as the difference between the threshold for spiking and the value of the membrane potential 5 ms after the potential returned to cross the threshold value at the end of the action potential. The spike amplitude was calculated as the difference between the maximum membrane potential during a spike and the threshold. Action potential width was calculated as the time it took the membrane potential to reach half the spike amplitude in the rising part of the spike to the descending part of the spike (Full Width at Half Maximum).

Input conductance

The input conductance was calculated around the resting membrane potential by measuring the current with the cell held in voltage clamp mode first at -70 mV and then at -50 mV. The difference in currents divided by the difference in membrane potential (of 20 mV) is the calculated input conductance.

Sodium and potassium currents

The sodium and potassium currents were acquired in voltage clamp mode. Cells were held at −60 mV, and voltage steps of 400 ms were made in the range of −90 mV to 80 mV. Currents were usually normalized by the cell capacitance (changing the units from pA to pA/pF), by an automatic Matlab script. In addition, when calculating the fast potassium currents at the low depolarization potentials (-20 mV to 20 mV), we manually calculated the currents because fluctuations that are due to the opening of the sodium currents (see for example Supplementary Fig. 9) affect the measurement with the automatic script, making them inaccurate in these potentials.

Fast and slow potassium currents

The fast potassium current has been shown to be related to the A-type potassium channels (Rudy, 1988). We measured the fast potassium current by the maximum current immediately following a depolarization step, typically within a time window of a few milliseconds. The slow potassium currents were obtained at the end of the 400-ms depolarization step and have been shown to be related to the delayed rectifier potassium channels (Rudy, 1988).

Kinetics of closing of sodium channels by inactivation

An exponential decay coefficient was fitted to the current curve during voltage clamp conditions at -20 mV from the minimum of the input current to the current 200 ms after the depolarization step. This decay coefficient was considered the kinetics time constant.

Kinetics of opening of sodium channels by depolarization

The time constant of the opening of the sodium currents was taken as the time from the depolarization step until the input current reached its minimum (at -20 mV)

Excitability graph as a radius of the dot

To see the dots at a reasonable size, the radius of each of the dots in the graph was plotted as the total number of evoked potentials to the exponent of 0.85.

Kinetics of closing of the fast potassium channels by inactivation

An exponential decay coefficient was fitted to the maximum outward current at 20 mV to the current at 200 ms after the voltage step. This decay coefficient was considered the kinetics time constant of the closing or the fast potassium currents.

Imaging of soma size

During electrophysiological recordings, the images of the neurons recorded were captured for later analysis of the soma size, which was done using ImageJ SW.

Tracing of neural progenitor cells (NPCs)

NPCs were plated on glass coverslips and fixed 24 hours after plating using 4% paraformaldehyde (PFA). Thirty cells were then imaged from each group and analyzed with Neurolucida SW, where neurites and soma were manually traced.

Channel blockers

Channel blockers were applied to the extracellular recording solution at the following concentrations: 1 mM tetraethylammonium chloride (TEA cat. 306850 R&D systems), 0.3 mM 4-aminopyridine (4-AP Tocris cat. 940100) and 200 nM α-dendrotoxin (DTX Bachem, cat. H-1088).

Immunohistochemistry

Cells were fixed in 4% paraformaldehyde for 15 minutes. Cells were subsequently blocked and permeabilized in PBS containing 0.1%–0.2% triton X-100 and 10% horse serum. Coverslips were incubated with primary antibody in blocking solution overnight at 4^{o} C, washed in Tris-buffered saline, incubated with secondary antibodies for 30 minutes at room temperature, counterstained with DAPI, washed, mounted on slides using PVA-DABCO (Sigma-Aldrich), and dried overnight protected from light. The following antibodies and dilutions were used: Map2ab (1:1000), Elavl2 (1:250), Elavl2/4 (1:500), Scgn (1:250, Invitrogen), NeuN (mouse, 1:100, Millipore), ELAVL2 (1:100), and GABA (1:1000). Fluorescence signals were detected using a Zeiss 710 confocal microscope and images were processed with Zen and ImageJ.

Results

CA3 pyramidal neurons derived from BD patients are hyperexcitable only when derived from patients with a good outcome in response to lithium treatment, and spike shape properties are altered between the three groups: control, LR and NR

Both DG and CA3 neurons were patch clamped at time point t2. We partitioned our data into 3 groups: neurons derived from control individuals, neurons derived from BD patients who responded to lithium (LR), and neurons derived from BD patients who did not respond to lithium (NR). Around 60% of the neurons in the 3 groups were CA3 pyramidal neurons, expressing the ELAVL2 protein (see Supplementary Figure 1a for immunohistochemistry and Supplementary Figure 1c for quantification of the number of neurons expressing the ELAVL2 protein, which is a specific marker for CA3 pyramidal neurons), and approximately 12% of the neurons were expressing GABA (see Supplementary Fig. 1b for representative images, and Supplementary Fig. 1d for quantification). The total number of action potentials produced in 35 first depolarization steps (see Methods) was counted, and this number served as the measure for excitability throughout this study. Unlike DG neurons, where both LR and NR DG neurons produced significantly more action potentials than the control neurons, only LR CA3 neurons produced significantly more evoked action potentials when compared to control CA3 neurons (Fig. 1a for averages and Fig. 1b-d for representative example recordings). This hyperexcitability of the LR CA3

neurons appeared in the form of the ability to sustain activity with high current injections (see Fig. 1e-g for representative traces with a 50 pA current injection). So LR neurons recovered faster from sodium inactivation periods and were therefore able to sustain activity in high current injections. Like DG LR neurons, LR CA3 neurons also exhibited a faster rate of spontaneous activity (when holding the cell at a potential of -45 mV in voltage clamp mode) (Fig. 1h). Similar to what we reported earlier (Stern et al., 2018), the spike shape features of DG and CA3 neurons were different between the 3 groups in the recording time t2 (a time point that is slightly different than the recording time in our previous study; see Methods). The fast AHP was increased in both LR and NR DG neurons, but only in LR CA3 neurons compared to the controls (Fig. 1i-k for example recordings, and Fig. 1l for averages). (The development over time is shown in Supplementary Fig. 2a for DG and CA3 neurons). The spike height was similarly larger for LR neurons both in DG and in CA3 neurons (Fig. 1m, Supplementary Fig. 2b); spike width was narrowest for LR CA3 neurons (Fig. 1n, Supplementary Fig. 2c), The threshold for evoking an action potential was more depolarized in NR DG neurons, with no significant changes in NR CA3 neurons (Fig. 1o, Supplementary Fig. 2d). The input conductance was increased in NR CA3 neurons (Fig. 1p, Supplementary Fig. 2e).

In the same recording period t2, which was half a week later on average than our previous study (Stern et al., 2018), we observed in DG neurons a hyperexcitability of both LR and NR BD neurons compared to controls. Generally, CA3 neurons of the control and LR groups produced more action potentials than DG control and LR groups (at the same age of the neurons), respectively, but CA3 NR neurons did not produce more action potentials than NR DG neurons (Supplementary Fig. 3a). DG granule neurons are inactive compared to other neuronal types in the hippocampus (Senzai and Buzsaki, 2017), and this may be the reason that in our experiments control and LR DG neurons are less excitable than control and LR CA3 neurons. Supplementary Figures 3b-3c show the number of evoked potentials at an earlier time point (t1=14-23 days after start of differentiation), and Supplementary Figure 3f shows the development over time of the evoked activity for DG and CA3 neurons. At t1, DG neurons already exhibited differences between the 3 groups, whereas, in CA3 neurons, the differences were not yet evident (Supplementary Fig. 3b). There was no significant difference between the spontaneous activity of DG and CA3 neurons in any of the 3 groups (Supplementary Fig. 3d for rate, and 3e for amplitude). Supplementary Figures 4 and 5 show different comparisons of the spike features in the 3 groups and over 2 differentiation times.

Excitability is correlated with the amplitude of fast potassium currents in BD hippocampal neurons, and blocking these currents diminishes the hyperexcitability phenotype

Trying to pinpoint what the changes in the BD neurons might be that contribute to the hyperexcitability phenotype, we compared some of the currents between the 3 groups. One of the currents that showed a significant difference in the BD neurons both in DG and CA3 neurons was the fast potassium current. A significant increase in amplitude of the fast potassium currents was measured. Figure 2a-b shows the amplitude of the fast potassium currents in CA3 and DG neurons at low depolarization potentials for the 3 groups, and it was increased in the BD neurons. Interestingly, the decay time for the fast potassium currents was also significantly faster in the LR CA3 neurons compared to CA3 neurons in the other groups, and slower in NR DG neurons compared to control DG (Fig. 2c and example traces in Fig. 2d), implying different ion channel distributions. Next, to see the effects of the amplitude and kinetics of the fast potassium currents, we plotted the excitability as proportional to the size of the circle (see Methods for exact mathematical formula) as a function of the amplitude of the fast potassium currents on the y axis, and as a function of the time constant of the decay of the fast potassium currents (see Methods) on the x axis for CA3 neurons (Fig. 2e) and DG neurons (Fig. 2f). The graphs show that control and LR CA3 neurons produced more action potentials than DG neurons (as seen also in Supplementary Fig. 3a). It is

known that mature DG neurons are very quiescent, but not mature CA3 pyramidal neurons, and this finding may be an indication of this phenomenon. In addition, BD CA3 neurons generally had larger amplitudes of the fast potassium currents than DG neurons. Neurons with the shorter and faster time constants were more excitable and, in DG neurons, the cells that were more excitable had larger amplitudes and faster kinetics of the fast potassium currents, as indicated by the larger circles in the left-upper parts of these graphs.

Holding the cells in a voltage clamp, we measured sodium currents (Fig. 2g for CA3 and Fig.2h for DG). CA3 NR neurons had significantly lower sodium currents (Fig. 2g sodium currents, and Supplementary Fig. 7i sodium currents normalized by capacitance) compared to CA3 LR and CA3 control ($p<0.0001$ for currents at -20 mV for the normalized currents). DG NR neurons also had lower sodium currents ($p=0.038$ for currents at -20 mV for the normalized currents). (Fig. 2h shows sodium currents, and Supplementary Fig. 7j shows sodium currents normalized by capacitance). Since the sodium channel opening happens in a positive feedback manner, probably due to the lower amplitudes of sodium currents, the sodium closing (Supplementary Figure 7c) and opening (Supplementary Figure 7d) kinetics were slower in CA3 NR neurons.

To further assess the affect that these changes in currents had on neuronal excitability, we calculated the correlations between the amplitude of the sodium currents and amplitude and kinetics of the fast potassium currents and excitability. We plotted the excitability as a function of the sodium currents at -20 mV holding potential (Fig. 2i-k). As expected, all 3 groups had a positive correlation between the amplitude of the fast potassium currents and the excitability ($R=0.37$. $p=0.004$ for control CA3 neurons, $R=0.33$, $0=0.027$ for LR CA3 neurons and $R=0.72$, $p=1e-11$ for NR CA3 neurons). Interestingly, there was also a significant correlation between the excitability and the amplitude of the fast potassium currents at 10 mV in the LR CA3 neurons (Fig. 2m, $R=0.31$, $p=0.04$) and in the NR neurons (Fig. 2n, $R=0.36$, $p=0.003$), but no correlation between the excitability of the control neurons and the amplitude of their fast potassium currents (Fig. 2l, $R=0.03$. $p=0.82$) was observed. When correlating with the time constant of decay of the fast potassium currents, there were also significant correlations, especially in the CA3 neurons. The correlation of the excitability and the time constant in all 3 groups pooled together was $R=-0.38$, $p=6e-5$ (so the faster the kinetics is, the more excitable the neuron is). In DG neurons this correlation was borderline significant, $R=-0.24$, $p=0.05$ (excitability and decay time in all 3 groups together). In DG in general, the decay time constants were faster compared to CA3 decay time, except in the LR group, as can be seen Figure 2c, 2e and 2f. Since the amplitude of the fast potassium currents was correlated with the BD neurons' excitability, we next blocked these currents using 3 different channel blockers - 200 nM dendrotoxin (DTX), 1 mM tetraethylammonium (TEA), and 0.3 mM of 4-aminopyridine (4-AP) - to look for the effect on neuronal excitability. The results are depicted in Figure 2o. Potassium blockers did not reduce the excitability of control neurons and application of DTX made the cells significantly more excitable. DTX was previously reported to increase excitability in rat neocortical pyramidal neurons (Bekkers and Delaney, 2001). However, potassium channel blockers reduced excitability in both LR and NR neurons. More specifically, all of them significantly reduced the hyperexcitability in LR neurons, with TEA having the largest effect. In NR neurons, 4-AP significantly reduced the excitability. We next performed qPCR for a few types of potassium channels. Kcnc1 was significantly overexpressed in LR neurons compared to control neurons ($p=0.005$) and an elevated level in the NR neurons that did not reach statistical significance compared to controls ($p=0.07$, Fig. 2p). Kcnc2 was also significantly overexpressed when comparing LR and control neurons ($p=0.01$, Fig. 2q), and NR neurons had a significant reduction in expression compared to controls ($p=0.04$). No change was observed in the expression of KCNMA1 and KCNMB1 genes (Supplementary Fig. 8a, 8b). Interestingly, fast spiking interneurons also had a strong expression of Kcnc1 and Kcnc2, and the high expression level of

these channels_was shown (Kaczmarek and Zhang, 2017; Martina et al., 1998) to assist with their fast spiking abilities, helping their fast recovery from sodium inactivation, similar to the physiology we observed for LR hippocampal neurons. After observing these changes in expression of the Kcnc genes in the CA3 neurons from this cohort, we re-analyzed our already published data (Mertens et al., 2015) and separated the cohort into 3 groups - control, LR and NR - to look at expression differences in the Kcnc genes. The results are plotted in Supplementary Figure 6. An overexpression of the Kcnc2 gene was observed in LR neurons. A similar overexpression of Kcnc3 was observed in LR neurons and a reduced expression in this gene was observed in the NR neurons. These Kcnc genes all belong to a family of very fast kinetics potassium channels. Supplementary Figure 7 presents the sodium and potassium currents (fast and slow) of DG and CA3 neurons of the 3 groups at 2 different differentiation time points, t1 and t2 (see Methods).

Neural progenitors, CA3 pyramidal and DG granule neurons are larger when derived from BD patients than from controls

In our previous study (Stern et al., 2018), we reported that DG neurons derived from BD patients were larger 3.5 weeks after starting differentiation from NPCs; specifically, the NR group neurons were the largest. We measured the capacitance at t2=4.5 weeks of CA3 pyramidal neurons (Supplementary Fig. 11a) and similarly observed that BD neurons were larger than controls and the NR group neurons were the largest (~30% increase in capacitance for the LR group, and 70% increase for the NR group when compared to the control group). The development course of the capacitance is shown in Supplementary Figure 11b. Imaging of the soma and tracing its size using ImageJ SW showed similar increases in cell size (Supplementary Fig. 11c). The ratio of capacitance to soma size was similar between the 3 groups (Supplementary Fig. 11d), indicating that there was a similar increase in neurite length and that the changes to the cell size in BD were scaled similarly throughout the entire cell. Example images of control, LR and NR CA3 neurons are provided in Supplementary Figure 11e-g. We were interested to see if these differences manifested as early as the NPC stage, so we imaged 75 control NPCs from the 4 patients, 60 LR NPCs (3 patients) and 60 NR NPCs (3 patients) and measured the soma size and the total neurite tree length. Interestingly, the soma was already larger in LR NPCs compared to controls, and even larger in NR NPCs (Supplementary Fig. 11h). The total neurite length was larger in the NR NPCs than in the controls (Supplementary Fig. 11i). Examples of control, LR and NR NPC images are shown in Supplementary Figure 11j-l.

Lithium increases sodium currents but reduces the amplitude of the fast potassium currents, resulting in a reduction of hyperexcitability of neurons derived from BD patients who respond to lithium (LR)

We were interested to see the effects of chronic lithium treatment on CA3 pyramidal neurons derived from patients and healthy subjects. We added 1 mM of LiCl to the media 2 weeks prior to patch clamp recordings, similar to the treatment that was used in our previous study (Stern et al., 2018). Lithium was not present during patch recordings. Similar to our previous reports on DG neurons (Stern et al., 2018), lithium reduced the hyperexcitability of CA3 neurons that were derived from LR patients. This effect was evident both in total evoked potential measurements (Fig. 3a) and spontaneous activity (Fig. 3b) but had little or no effect on the excitability of NR and control neurons. Interestingly, chronic lithium treatment reduced the size of the overly large neurons to a size that was more similar to the control neurons, both in LR and NR cells (Fig. 3c). By imaging and tracing the neurons during the electrophysiological recordings, we found that this change did not come from changes to the soma size (Fig. 3d); therefore, it likely emerged from the neurites' length and arborization. Looking further into spike parameters, we found that lithium treatment reduced spike height in LR neurons (Fig. 3e), did not change the fast AHP

significantly in any of the groups (Fig. 3f), broadened the spike in LR neurons (Fig. 3g), and did not alter the threshold for evoking an action potential in any of the groups (Fig. 3h). An increase in the normalized sodium currents was observed in all 3 groups (using an ANOVA. p=2e-4 for control, p=4e-8 for LR and p=3e-8 for NR) (Fig. 3i-k). There were no significant differences in the potassium currents in any of the 3 groups when we ran an ANOVA on the entire or part of the voltage recording range (Fig. 3l-q).

However, when comparing the amplitude of potassium currents at specific holding potentials with a t-test, we did find significant differences between the groups. We were therefore interested to see which of the holding potentials produced currents that correlated most with excitability (in continuation with the plots presented in Fig. 2i-k, 2l-n). We calculated the correlation of the cell excitability (as measured by the total amount of evoked potentials) and a few of the features and currents that were measured in the cell. The excitability generally correlated with capacitance for control and LR neurons (Supp. Fig. 12a-b), whereas it did not correlate with capacitance in NR neurons (Supp. Fig. 12c). This miscorrelation of excitability specifically in NR neurons with capacitance was already reported in our previous study with DG neurons (Stern et al., 2018). In LR neurons, where we have seen that lithium treatment reduced capacitance, the correlation grew stronger between excitability and capacitance after lithium treatment. Only in NR untreated neurons did the excitability correlate with the slow potassium currents (Supp. Fig. 12d-f). In LR and NR neurons, the excitability correlated much more strongly with the fast potassium currents at the lower depolarization steps (Supp. Fig. 12g-i) than with the fast potassium currents at the higher depolarization steps (Supp. Fig. 12j-l). And finally, as expected, the excitability correlated with the amplitude of the sodium currents. The very strong correlation for the NR neurons (R=0.72, p=1e-11) and the large slope of the line representing excitability as a function of sodium currents in NR neurons were notable (Supp. Fig. 12m-o). Since the correlation plots indicated that the fast potassium currents at the lower depolarization steps were more correlated with excitability in BD neurons, we also plotted the changes to these currents after lithium treatment. We observed that these currents were reduced in LR neurons after treatment (Fig. 3r), which is a possible cause of the reduction in excitability after lithium treatment. In addition, measurements of the decay time constants of the fast potassium currents showed that they were faster in control and NR neurons after lithium treatment, indicating faster kinetics (Fig. 3+s).

To summarize, lithium affected the cells in several ways. It reduced the huge capacitance of BD neurons. It increased the amplitude of the sodium currents in all 3 groups, and it reduced the amplitude of the fast potassium currents at the lower depolarization holding potential in the LR group (currents that we have showed correlate with excitability). We therefore think that this may be lithium's dual way of operation as a mood stabilizer: increasing sodium currents and thus reducing the amount of hypoexcitable cells on one hand, but also reducing the fast potassium currents and thus reducing the total number of hyperexcitable cells.

Motor neurons

Observing what seemed to be a multi-regional hyperexcitability of BD hippocampal neurons, we were interested to see whether a completely different, non-CNS neuron would show any different phenotype or physiology in BD. We differentiated our iPSCs into spinal motor neurons using the protocol previously described in our lab (Marchetto et al., 2008). Neurons were cultured on spinal astrocytes as described in the Methods section. Whole cell patch clamp was performed 10 days after dissociation of the neurospheres. Immunostaining for islet-positive cells (examples in Fig. 4a, 4b and 4c) indicated similar ratios of Islet+/MAP2 (Fig. 4d). To measure excitability, the total number of evoked potentials in 35 depolarization steps was measured, similar to the excitability measure that was used for DG and CA3 pyramidal neurons. There were no significant changes in the excitability between the 3 groups: control,

LR and NR (Fig. 4e). The spike parameters that were measured in hippocampal neurons - fast AHP (Fig. 4f), spike width (Fig. 4g), threshold (Fig. 4h) and spike amplitude (Fig. 4I) - were not significantly different between the 3 groups. There were no significant changes in capacitance (Fig. 4j) or in the input conductance (Fig. 4k) between the groups. Interestingly, sodium currents were increased in the NR neurons compared to the control neurons (using an ANOVA, p=5e-9, Fig. 4l). There was no significant change in the slow or fast potassium currents (Fig. 4m, 4n). To summarize, there were almost no physiological changes between the motor neurons of the 3 groups.

Discussion

BD affects approximately 2% of the worldwide population and puts a huge burden on the world's health and economic systems. This disorder was described first in detail in 2 books in the first century AD by Aretaeus of Cappadocia: "On the Aetiology and Symptomatology of Chronic Diseases" and "The Treatment of Chronic Diseases." In the 17th century, Theophilus Bonet described it in his work "Sepuchretum," where he linked mania and melancholy in a condition called "manico-melancolicus." Yet, after centuries of studying this condition, we still know very little about it. The introduction of iPSC technology allowed us for the first time to study this disorder in a dynamic human model and has enabled us to define an endophenotype of this disorder in the form of hippocampal overexcitability (Mertens et al., 2015; Stern et al., 2018) or, more specifically, DG hyperexcitability. Exciting as this step was, it only gave us the end of a thread that we could follow. So, having developed a new protocol for CA3 pyramidal neurons (Sarkar et al., 2018), we were interested to see if there were any functional changes in other types of hippocampal neurons; furthermore, we were interested in looking for the mechanisms that caused this hyperexcitability.

The phenotype of the CA3 pyramidal neurons that we report here was somewhat different than that of DG neurons. While BD DG neurons were hyperexcitable, only BD CA3 neurons derived from LR patients were hyperexcitable in our recordings. This hyperexcitability significantly correlated with the amplitude and the fast kinetics of their fast potassium currents. Moreover, qPCR experiments confirmed an overexpression of the fast kinetics potassium channels Kcnc1 and Kcnc2, which are known to assist fast spiking interneurons with their fast spiking ability. These changes had implications for their spike shape parameters: the spike amplitude was increased, the fast AHP was larger, and the spike width was narrower. Importantly, blocking these currents using different types of potassium channel blockers diminished the hyperexcitability phenotype, with the strongest effect seen using TEA. The NR CA3 neurons did not have a significantly increased excitability compared to the control CA3 neurons. However, their physiology had alterations that did not result in an average change in excitability of the cells: they had drastically reduced sodium currents and increased fast and slow potassium currents, but with a slower kinetics than the CA3 LR neurons. In the NR neurons, potassium channel blockers also reduced their excitability, with the strongest effect seen with 4-AP. Morphological analysis of the BD neurons showed that, as we previously reported for DG neurons, BD neurons were larger. Specifically, the BD NR neurons were very large (70% increase compared to controls). Interestingly, when we looked at NPCs, we also observed enlarged cell sizes for the LR and even more so for NR NPCs compared to the control NPCs. Reviewing the literature we found reports of enlarged (Beyer et al., 2004; Brambilla et al., 2003; Cao et al., 2016; Javadapour et al., 2010; Strakowski et al., 1999), smaller (Blumberg et al., 2003), and unchanged (Videbech and Ravnkilde, 2004) hippocampal volume in BD patients. However, there were also reports showing that multiple episodes of mania and depression correlated with this decrease in brain volume (Cao et al., 2017; Javadapour et al., 2010; Strakowski et al., 2002). Another interesting study showed that hippocampal volume was increased in BD patients and then decreased with the episodes' occurrence (Blumberg et al., 2003) It is therefore hard to know what the anatomical or

morphological changes in the patient's hippocampus before disease onset and episodes were. Thus the ability to model young hippocampal neurons from BD patients allows us to observe the morphology and function of BD hippocampal neurons before disease onset or any drug treatment, and we know now that BD hippocampal neurons are larger.

We have shown here a few lines of evidence supporting a conclusion that the hyperexcitability of LR hippocampal neurons is caused by an overabundance of very fast potassium channels, namely Kcnc1 and Kcnc2, thus resembling the physiology of fast spiking interneurons. We have shown with patch clamp experiments that there is an increased amplitude and faster kinetics of the fast potassium currents in LR neurons, and that the hyperexcitability correlated with the amplitude and kinetics of these currents. The fast AHP amplitude was increased in LR hippocampal neurons, which also points to the fast potassium currents, and also a phenotype that is similar to the fast spiking interneurons. With qPCR we have shown a gene overexpression of Kcnc1 and Kcnc2, and experiments using channel blockers targeting these fast potassium currents reduced the hyperexcitability drastically.

Lithium, being the first line of treatment of BD today, is known to be a mood stabilizer. Chronic lithium treatment in our neuronal cultures of 1 mM LiCl reduced the hyperexcitability of DG LR neurons (but not of DG NR neurons) (Stern et al., 2018) and reduced the hyperexcitability of CA3 LR neurons, as we show in this study. The treatment increased the sodium currents in all 3 groups (control, LR and NR) and decreased the amplitude of the fast potassium currents in the LR group. We hypothesize that this may be the dual mechanism by which lithium acts both to reduce depression episodes in patients on one hand (the increase in sodium currents) and to reduce mania episodes in patients on the other (the decrease of the amplitude of the fast potassium currents that correlates with the CA3 LR hyperexcitability, as we have shown in this study). It is also interesting to note the effect of lithium treatment on the reduction in cell capacitance both for the LR and NR groups in the CA3 neurons, as we had previously reported in the DG neurons (Stern et al., 2018). Lithium treatment in human patients has been shown to increase hippocampal volume, which may seem to contradict our results. However, there are also quite a few studies showing that reduction in hippocampal volume without treatment is due to recurrent episodes of mania and depression, which is likely why lithium causes a hippocampal volume increase (Hajek et al., 2012; Zung et al., 2016) in the patients.

To summarize, in this study, we unraveled some of the physiological changes in BD hippocampal neurons. Many previous studies have shown that BD manifests in the hippocampus (Blumberg et al., 2003; Fatemi et al., 2000), but it is important to keep in mind that other areas of the brain have also been shown to be affected (Abe et al., 2015; Altshuler et al., 1998; Hibar et al., 2018; Lawrence et al., 2004; Rajkowska et al., 2001), and further studies of other neuronal types should follow. We have shown here that BD motor neurons do not display any physiological changes compared to controls. LR neurons had larger fast potassium currents with a faster kinetics that significantly correlated with their hyperexcitability in the experiments. This hyperexcitability was accompanied by an overexpression of Kcnc1 and Kcnc2 genes, known to assist fast spiking interneurons with their fast spiking abilities. NR neurons had larger slow and fast potassium currents but with slower kinetics and had decreased sodium currents, but the NR CA3 neurons were not significantly hyperexcitable. BD neurons were also physically larger than control neurons. The increase in the amplitude of the potassium currents that underlies the phenotype of BD neurons can be blocked, reversing the phenotype. These blockers should be considered as an alternative treatment for BD (TEA seems most suitable for BD LR and 4-AP for BD NR), and we suggest their use for further studies with human subjects.

Figures

Figure 1

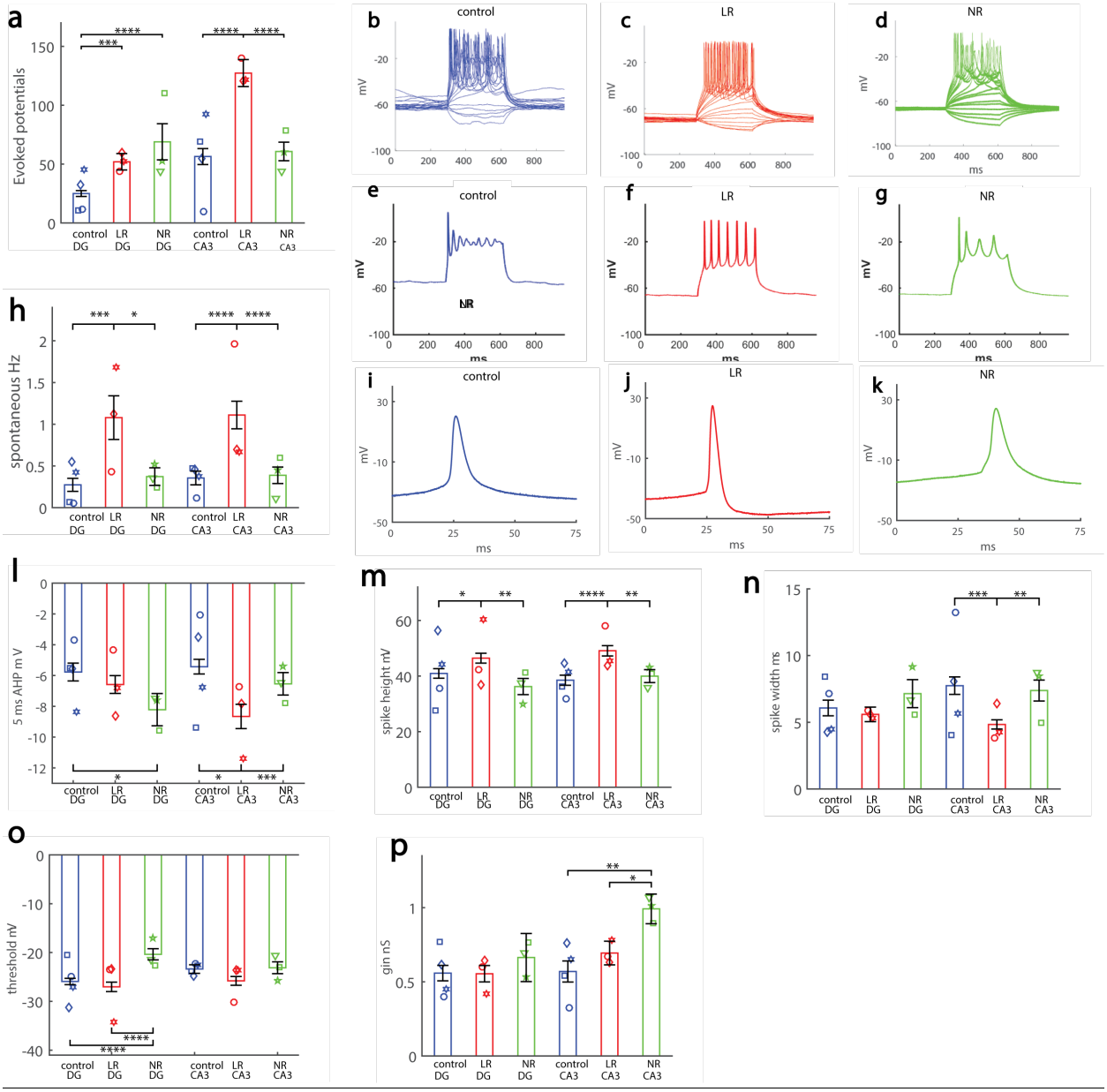

Figure 2

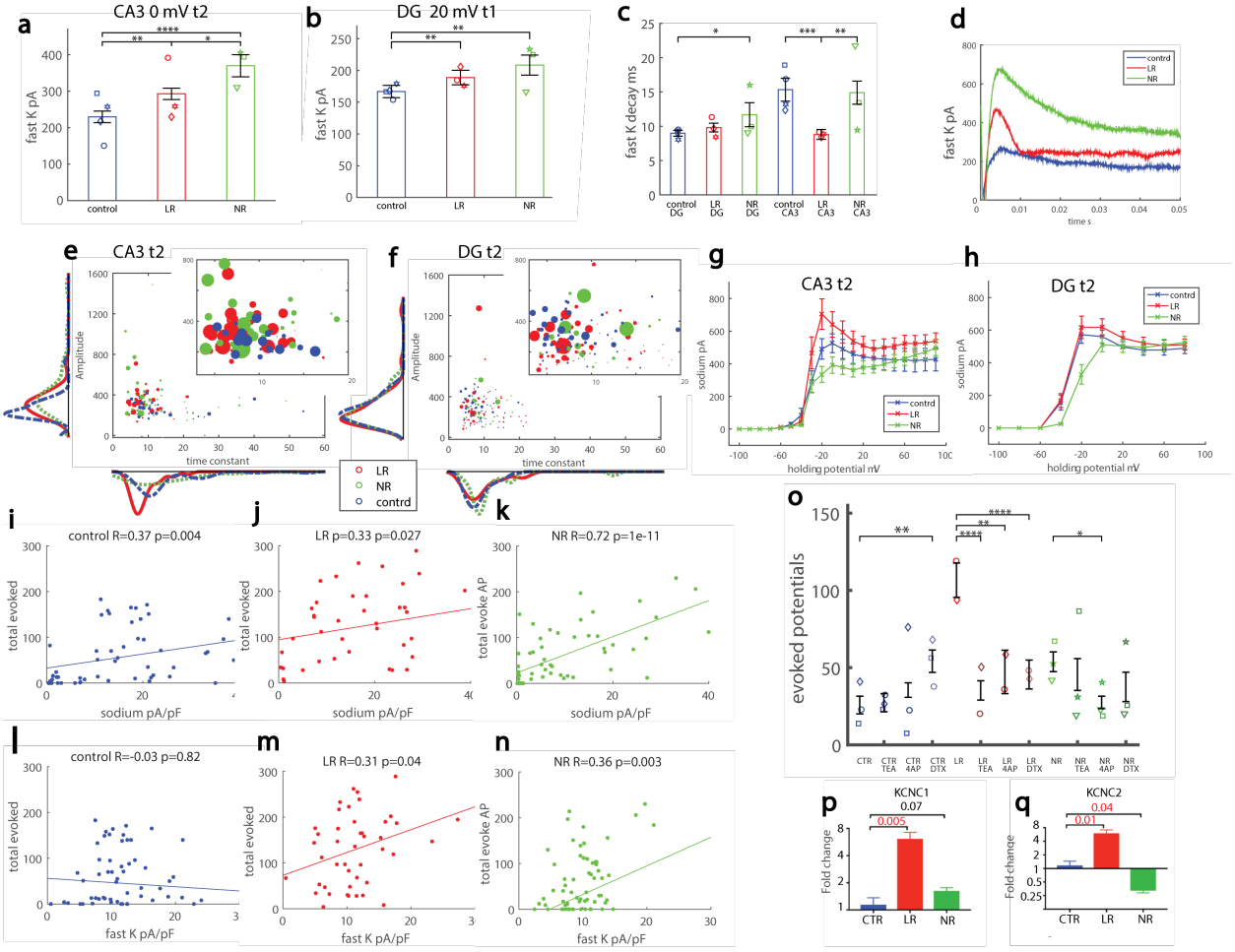
a
CA3 0 mV t2
fast K pA
control
LR
NR
b
DG 20 mV t1
fast K pA
c
fast K decay ms
control DG
LR DG
NR DG
control CA3
LR CA3
NR CA3
d
fast K pA
contrd
LR
NR
time s
e
CA3 t2
Amplitude
time constant
f
DG t2
g
CA3 t2
sodium pA
holding potential mV
h
DG t2
i
control R=0.37 p=0.004
total evoked
sodium pA/pF
j
LR p=0.33 p=0.027
k
NR R=0.72 p=1e-11
total evoke AP
l
control R=-0.03 p=0.82
fast K pA/pF
m
LR R=0.31 p=0.04
n
NR R=0.36 p=0.003
o
evoked potentials
CTR
CTR TEA
CTR 4AP
CTR DTX
LR
LR TEA
LR 4AP
LR DTX
NR
NR TEA
NR 4AP
NR DTX
p
KCNC1
0.07
0.005
Fold change
q
KCNC2
0.04
0.01

Figure 3

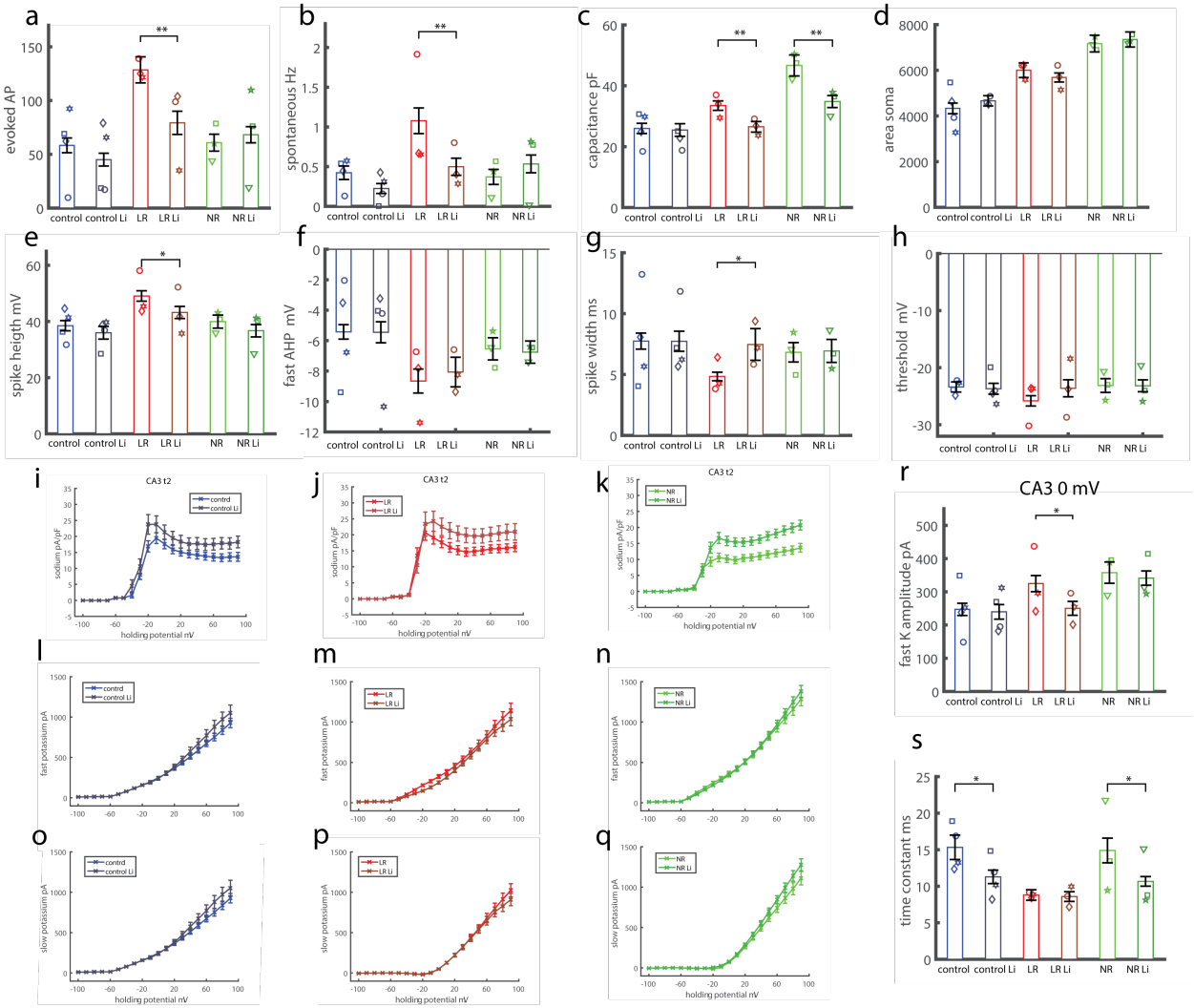
a
evoked AP
b
spontaneous Hz
c
capacitance pF
d
area soma
e
spike heigth mV
f
fast AHP mV
g
spike width ms
h
threshold mV
control control Li LR LR Li NR NR Li
i
CA3 t2
control
control Li
sodium pA/pF
holding potential mV
j
CA3 t2
LR
LR Li
k
CA3 t2
NR
NR Li
r
CA3 0 mV
fast K amplitude pA
l
fast potassium pA
m
n
o
slow potassium pA
p
q
s
time constant ms

Figure 4

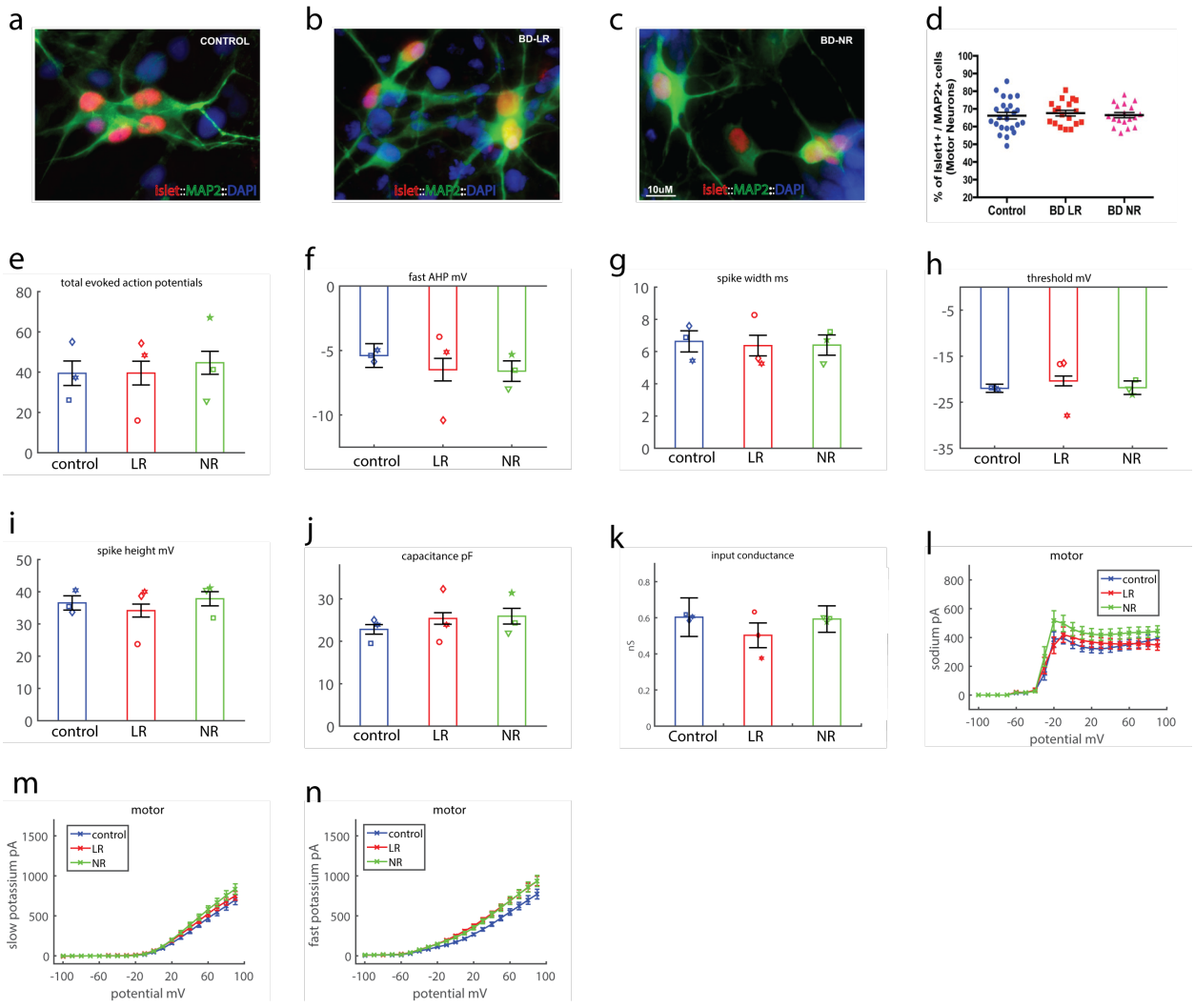
a
CONTROL
Islet::MAP2::DAPI
b
BD-LR
Islet::MAP2::DAPI
c
BD-NR
10uM
Islet::MAP2::DAPI
d
% of Islet1+ / MAP2+ cells (Motor Neurons)
Control
BD LR
BD NR
e
total evoked action potentials
control
LR
NR
f
fast AHP mV
control
LR
NR
g
spike width ms
control
LR
NR
h
threshold mV
control
LR
NR
i
spike height mV
control
LR
NR
j
capacitance pF
control
LR
NR
k
input conductance
nS
Control
LR
NR
l
motor
control
LR
NR
sodium pA
potential mV
m
motor
control
LR
NR
slow potassium pA
potential mV
n
motor
control
LR
NR
fast potassium pA
potential mV

Figure legends

Figure 1. Hyperexcitability in hippocampal neurons derived from BD patients a. Cells patched at 30 days from start of differentiation. DG BD LR and NR neurons are hyperexcitable when compared to controls, but only BD LR CA3 neurons are hyperexcitable compared to controls. The points that were plotted represent the mean of each cell line (patient), but the number of total neurons patched is as follows: DG: control n=76 neurons, LR n=69 neurons, NR n=25 neurons; CA3: control n=58 neurons, LR n=46 neurons, NR n=71 neurons. b. Representative example recordings in current clamp mode of evoked potentials for a control (blue), c. LR (red) and d. NR (green) neuron. Plotting only the high current injection component reveals that the hyperexcitability of LR neurons was in the form of sustained activity with high current injections, as can be seen from the representative traces of the e. control (blue), f. LR (red) and g. NR (green) CA3 neurons. h. Spontaneous activity. BD LR neurons have an increase in the rate of spontaneous activity both in DG and CA3 neurons. Analysis of spike shape. i. Example recordings of a single spike in current clamp mode of a control (blue) neuron, j. LR (red) neuron and k. NR (green) neuron. l. The fast after-hyperpolarization (AHP) is increased in the BD NR DG neuron at the t2 time point. Our previous report at t* (around 25 days after start of differentiation) (Stern et al., 2018) showed that DG LR fast AHP was also increased at that time point. Fast AHP is also increased in BD LR CA3 neurons. m. Spike amplitude is larger for BD LR neurons, both in DG and CA3, when compared to control and NR neurons. n. Spike width is narrower in CA3 LR neurons. In (Stern et al., 2018), at the t* time point, DG LR neurons also displayed a narrower spike width. o. The threshold for eliciting an action potential is more depolarized in DG NR neurons compared to control and BD LR neurons, but there is no significant change between the 3 groups in CA3 neurons. p. Input conductance is larger in CA3 BD NR neurons compared to control and BD LR neurons. Asterisks represent statistical significance by the following code: * p value<0.05, **p value<0.01, ***p<0.001, ****p<0.0001. Error bars represent standard error.

Figure 2. The effects of different currents on cell excitability. Each dot in the graphs represents an average over the total amount of patched cells for one human subject. a. The manual measurement of fast potassium currents in CA3 neurons at 0 mV (see Methods section) shows a significant increase in BD LR and even more in BD NR. b. Similarly, in DG at 20 mV, BD LR neurons have increased fast potassium currents and BD NR neurons have an even more elevated level. c. Fast potassium decay time. In DG, NR neurons have a slower kinetics compared to control neurons. In CA3, LR neurons have a very fast kinetics compared to control and NR neurons. d. Representative example recordings of CA3 control (blue), LR (red) and NR (green) neurons in voltage clamp mode, displaying the increased amplitude of the fast potassium currents in BD LR and BD NR neurons and the faster kinetics in BD LR neurons. e. CA3 excitability (encoded in the radius of the dot, see Methods) as a function of the amplitude of the fast potassium currents (y-axis) and the kinetics or decay time constant of the fast potassium current (x-axis). The larger dots are generally observed in the neurons with fast kinetics or fast decay time of the fast potassium currents. f. DG excitability (encoded in the radius of the dot, see Methods) as a function of the amplitude of the fast potassium currents (y-axis) and the kinetics or decay time constant of the fast potassium current (x-axis). The larger dots are observed in the neurons with fast kinetics or fast decay time and higher amplitudes of the fast potassium currents. g. Sodium currents are reduced in CA3 NR neurons compared to controls and increased in CA3 LR neurons compared to controls. h. Sodium currents are reduced in DG NR neurons compared to controls and slightly increased in DG LR neurons compared to controls. i-k. The excitability in all the groups correlate with sodium currents (at -20 mV). This correlation is much stronger in NR neurons compared to control and LR neurons. l-n. A significant

correlation is observed between excitability and the amplitude of the fast potassium currents at 0 mV in LR and NR neurons. The excitability in control neurons does not correlate with the amplitude of the fast potassium currents at 0 mV. o. Blocking of different potassium channels reduced excitability of CA3 BD neurons but increased excitability of CA3 control neurons; Dendrotoxin (DTX) at 200 nM significantly increased excitability of control neurons. 1 mM Tetraethylammonium (TEA) most drastically reduced hyperexcitability of CA3 LR neurons, but 0.3 mM of 4-aminopyridine (4-AP) and DTX also significantly reduced their hyperexcitability. 4-AP reduced excitability of CA3 NR neurons. A total number of 53 control, 28 control TEA, 27 control 4-AP, 28 control DTX, 47 LR, 39 LR TEA, 18 LR 4-AP, 29 LR DTX, 104 NR, 28 NR TEA, 28 NR 4-AP and 28 NR DTX neurons were recorded. p. qPCR results (fold change) of Kcnc1 showed that CA3 LR neurons have elevated levels compared to control neurons. q. Fold change values of Kcnc2 showed a decreased expression in NR neurons and an increased expression in LR neurons compared to CA3 control neurons. Asterisks represent statistical significance by the following code: * p value<0.05, **p value<0.01, ***p<0.001, ****p<0.0001. Error bars represent standard error.

Figure 3. Response to lithium treatment of CA3 neurons at t2. The total number of cells patched for this analysis was as follows: control, n=49 neurons; control lithium (Li), n=56 neurons; LR, n=43 neurons; LR Li, n=41 neurons; NR, n=71 neurons; NR Li, n=65 neurons. a. Lithium treatment reduces the hyperexcitability (total number of evoked action potentials) of CA3 BD LR neurons. b. The spontaneous rate of action potentials is also reduced with lithium treatment in CA3 BD LR neurons. c. Similar to our previous report in DG neurons (Stern et al., 2018), the capacitance of BD LR and BD NR neurons is smaller with lithium treatment than the equivalent neurons grown without treatment. d. The soma of the BD LR and BD NR CA3 neurons did not decrease in size with lithium treatment, indicating that the reduction in capacitance with lithium treatment was due to a reduction in size of the neuritic tree. e. The spike height of BD LR CA3 neurons was reduced with lithium treatment. f. The fast AHP did not change with lithium treatment in any of the groups. g. The spike width broadened after lithium treatment in CA3 BD LR neurons. h. The threshold for evoking an action potential did not change in any of the 3 groups following lithium treatment. i. Lithium treatment increased normalized sodium currents in control CA3 neurons. j. Lithium treatment increased normalized sodium currents in BD LR CA3 neurons. Lithium treatment increased normalized sodium currents in BD NR CA3 neurons. l-q. The fast and slow potassium currents did not change significantly (ANOVA). r. The amplitude of the fast potassium current at 0 mV was significantly decreased after lithium treatment in CA3 BD LR neurons. s. The decay time constant of the fast potassium current decreased (decay was faster) with lithium treatment in CA3 control and CA3 BD NR neurons. Each dot represents an average over the total number of patched cells for one human subject. Asterisks represent statistical significance by the following code: * p value<0.05, **p value<0.01. Error bars represent standard error.

Figure 4. Physiology of motor neurons in BD a. Example image of control islet-positive neurons. b. Example image of LR islet-positive neurons. c. Example image of NR islet-positive neurons. d. Similar ratios of islet-positive neurons in the 3 groups. e. Neurons from the 3 groups display similar excitability measured by the total number of elicited action potentials. Spike parameters: fast AHP (f), spike width (g), threshold (h) and spike height (i) are similar between the 3 groups. j. Capacitance is similar between the 3 groups. k. Input conductance is similar between the 3 groups. l. Sodium currents are similar between the 3 groups. m. Slow potassium currents are similar between the 3 groups. n. The fast potassium current is similar between the 3 groups. Each dot represents an average over the total number of patched cells for one human subject.

Supplementary Figure 1

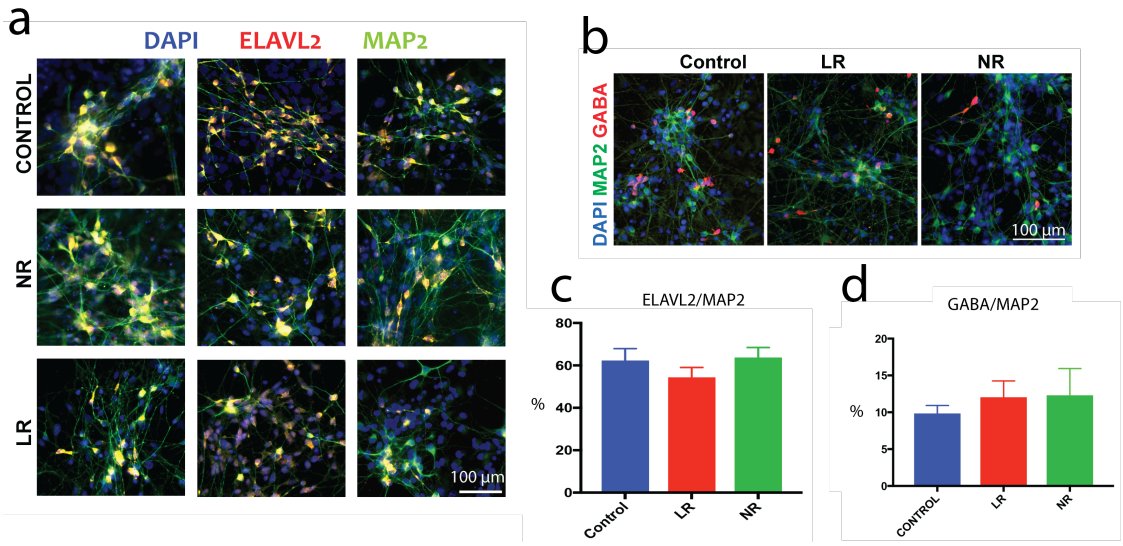

Supplementary Figure 2

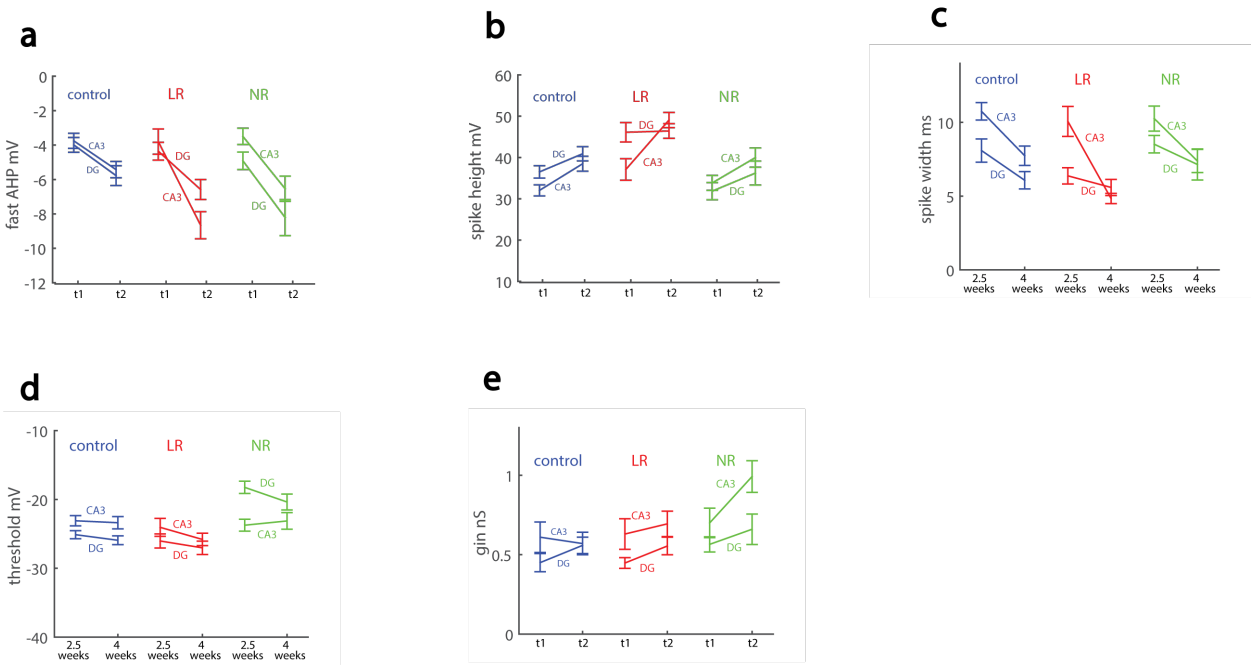

Supplementary Figure 3

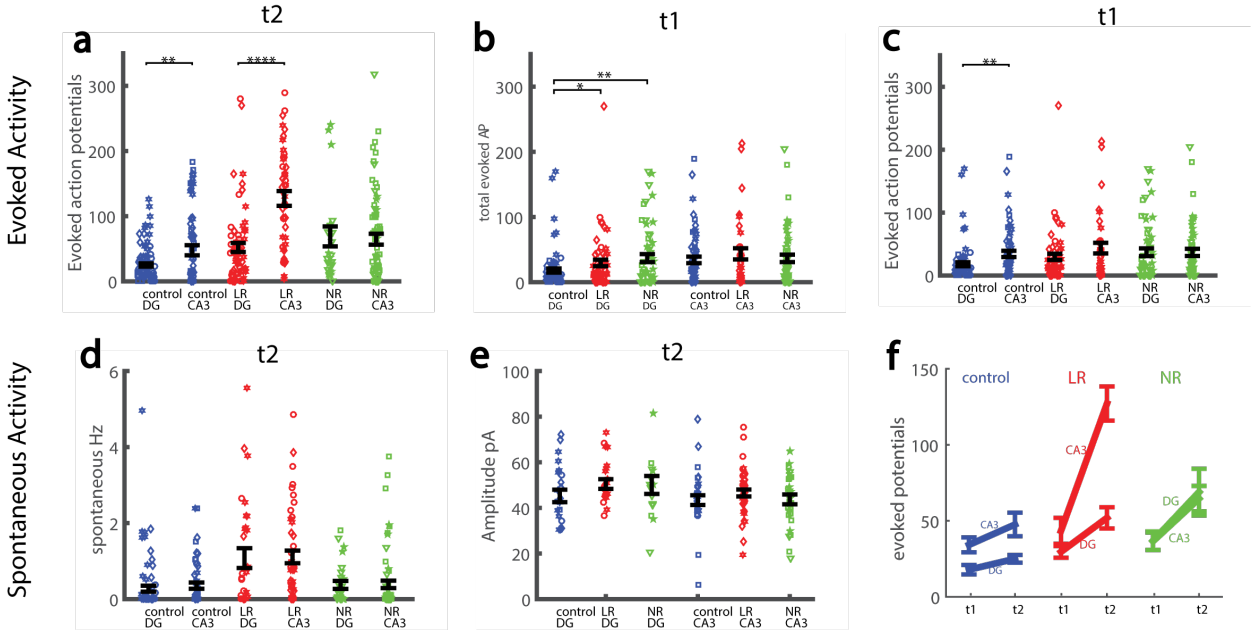

Supplementary Figure 4

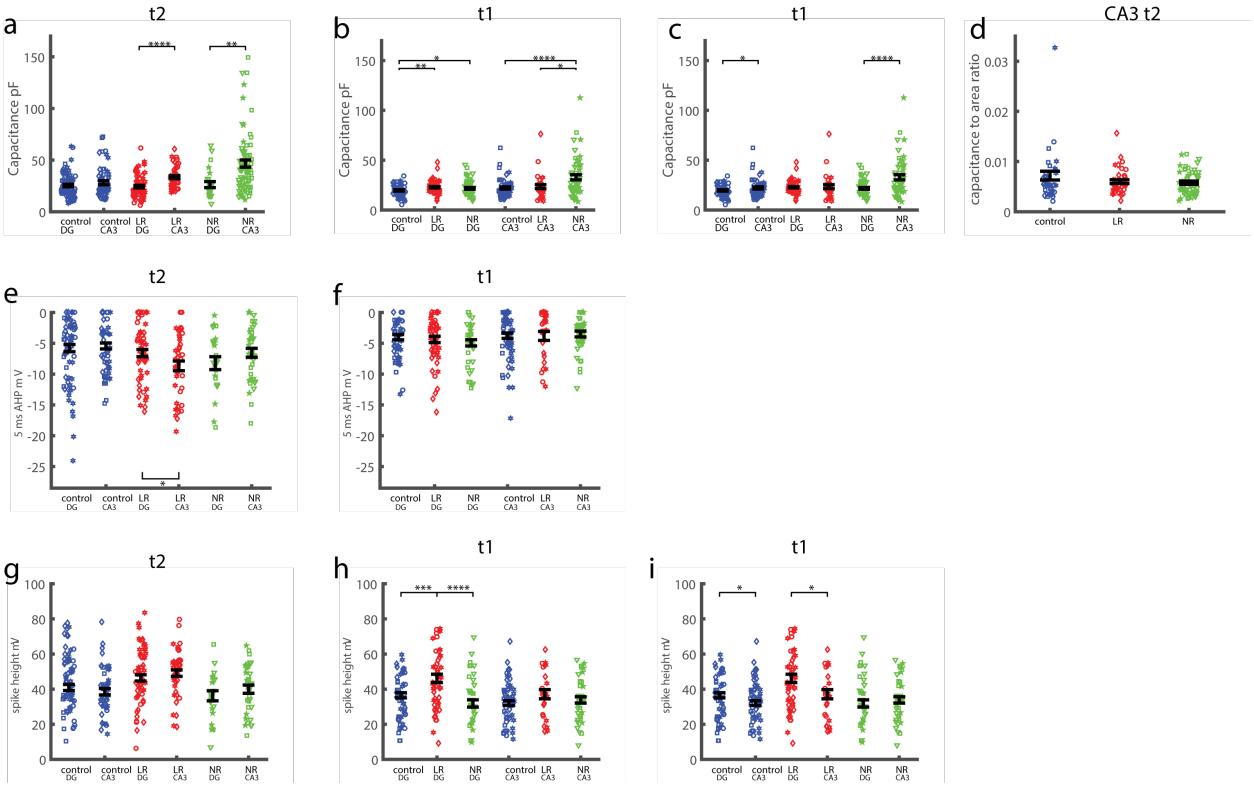

Supplementary Figure 5

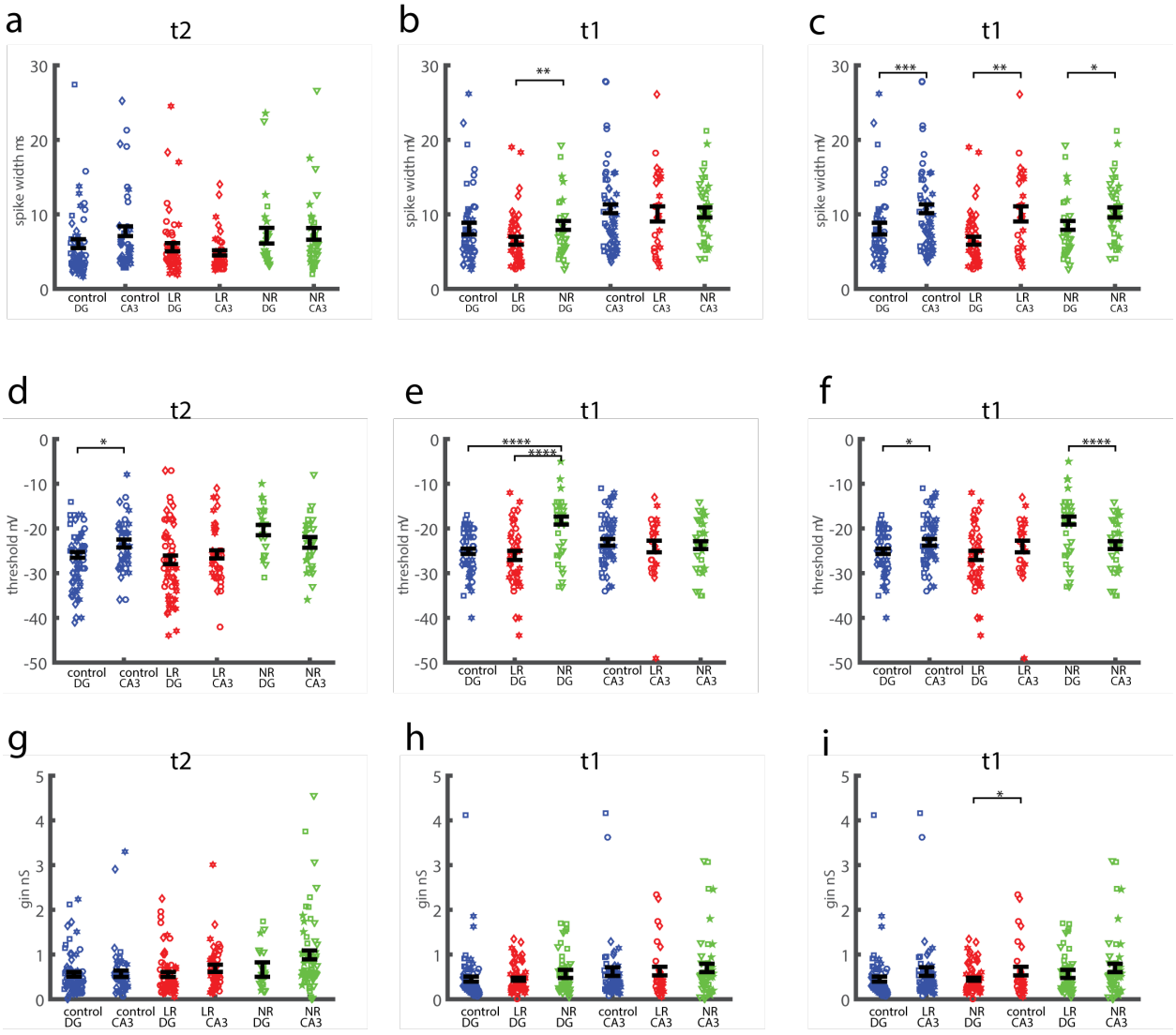

Supplementary Figure 6

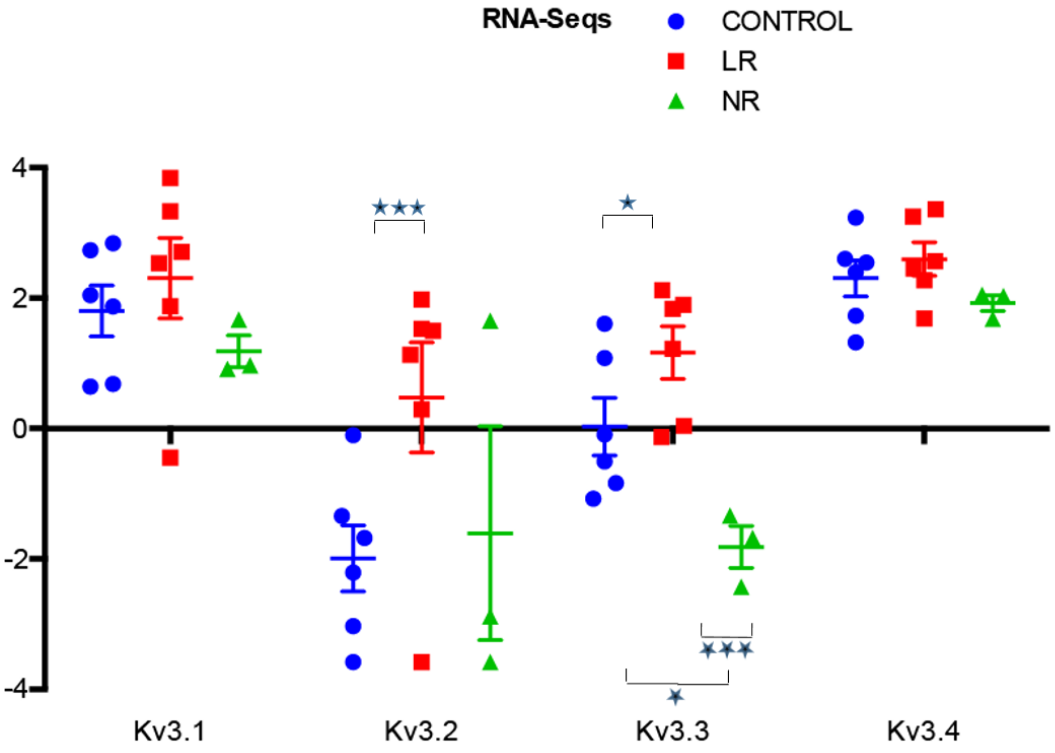

Supplementary Figure 7

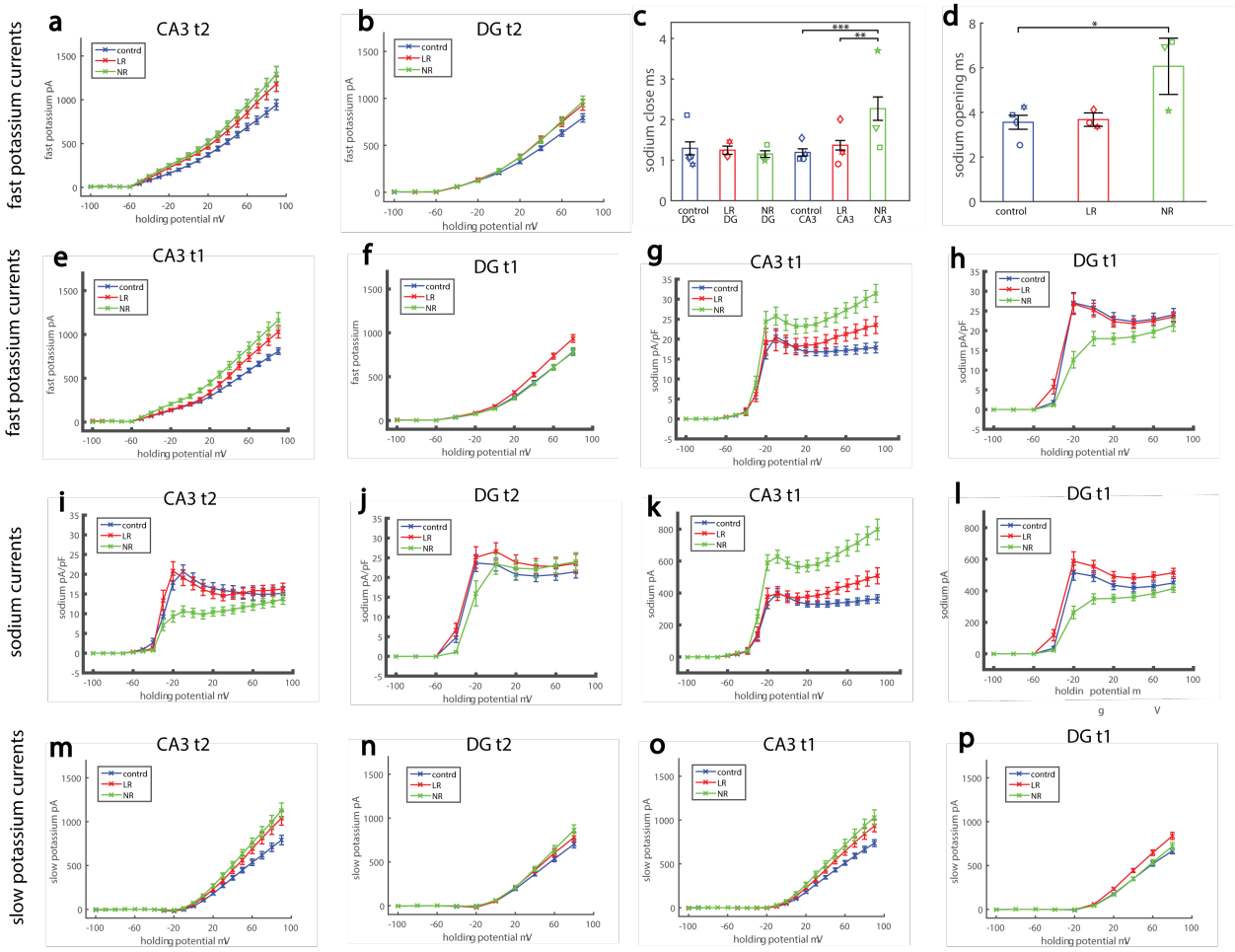

Supplementary Figure 8

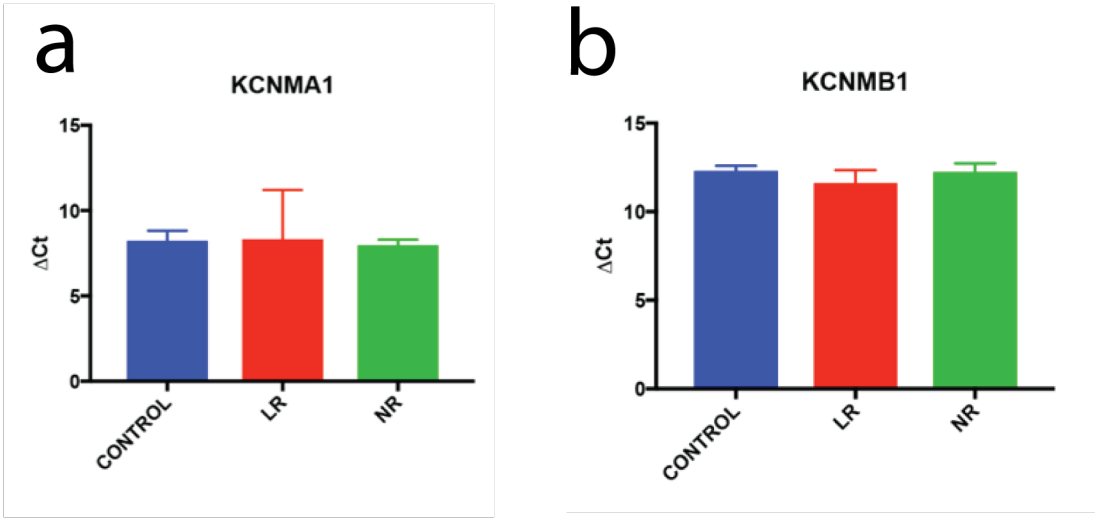

Supplementary Figure 9

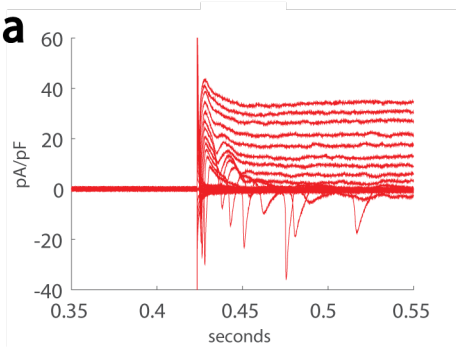

Supplementary Figure 10

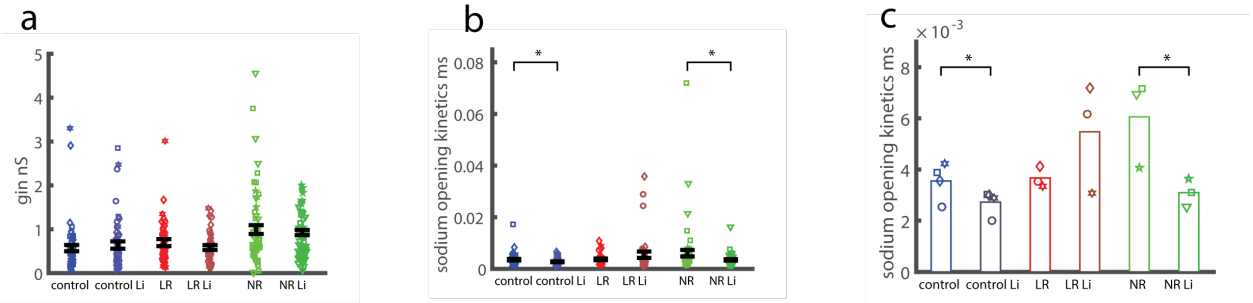

Supplementary Figure 11

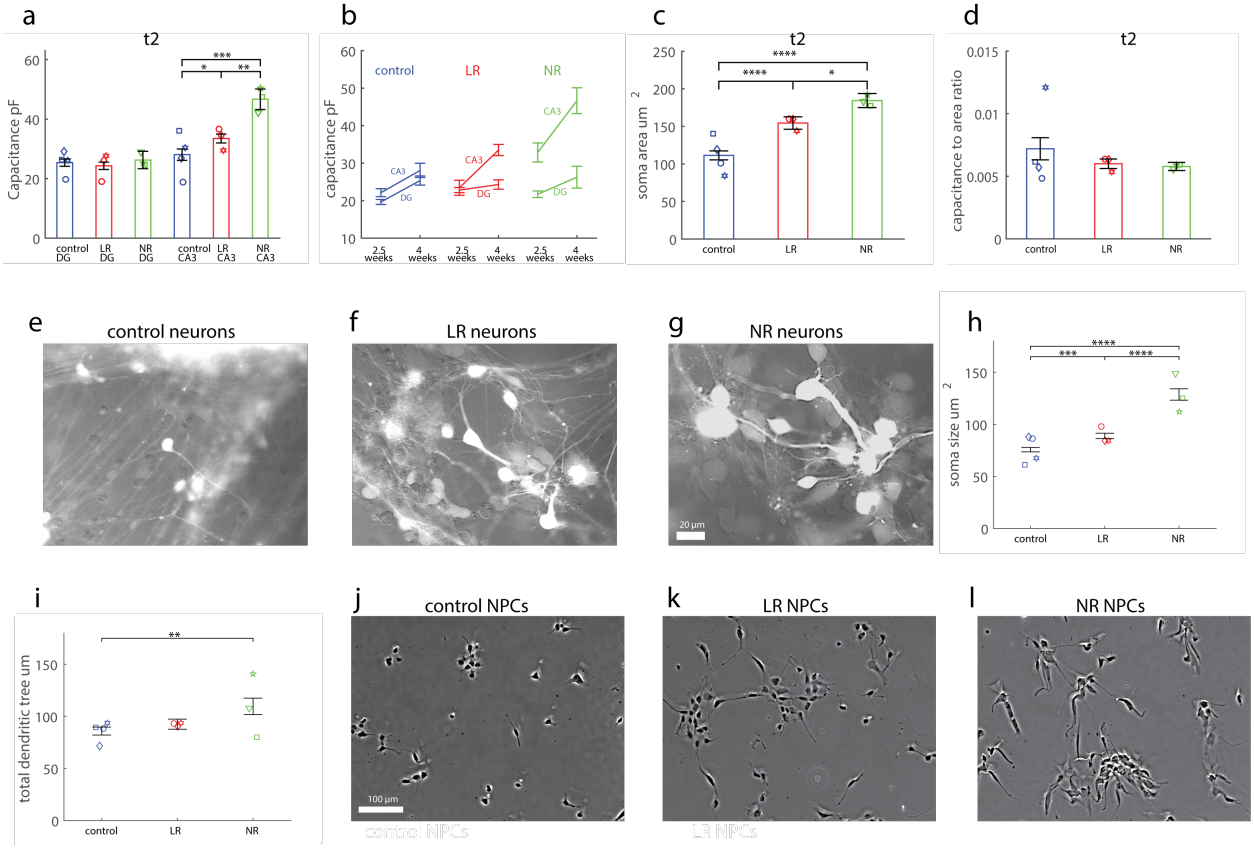

Supplementary Figure 12

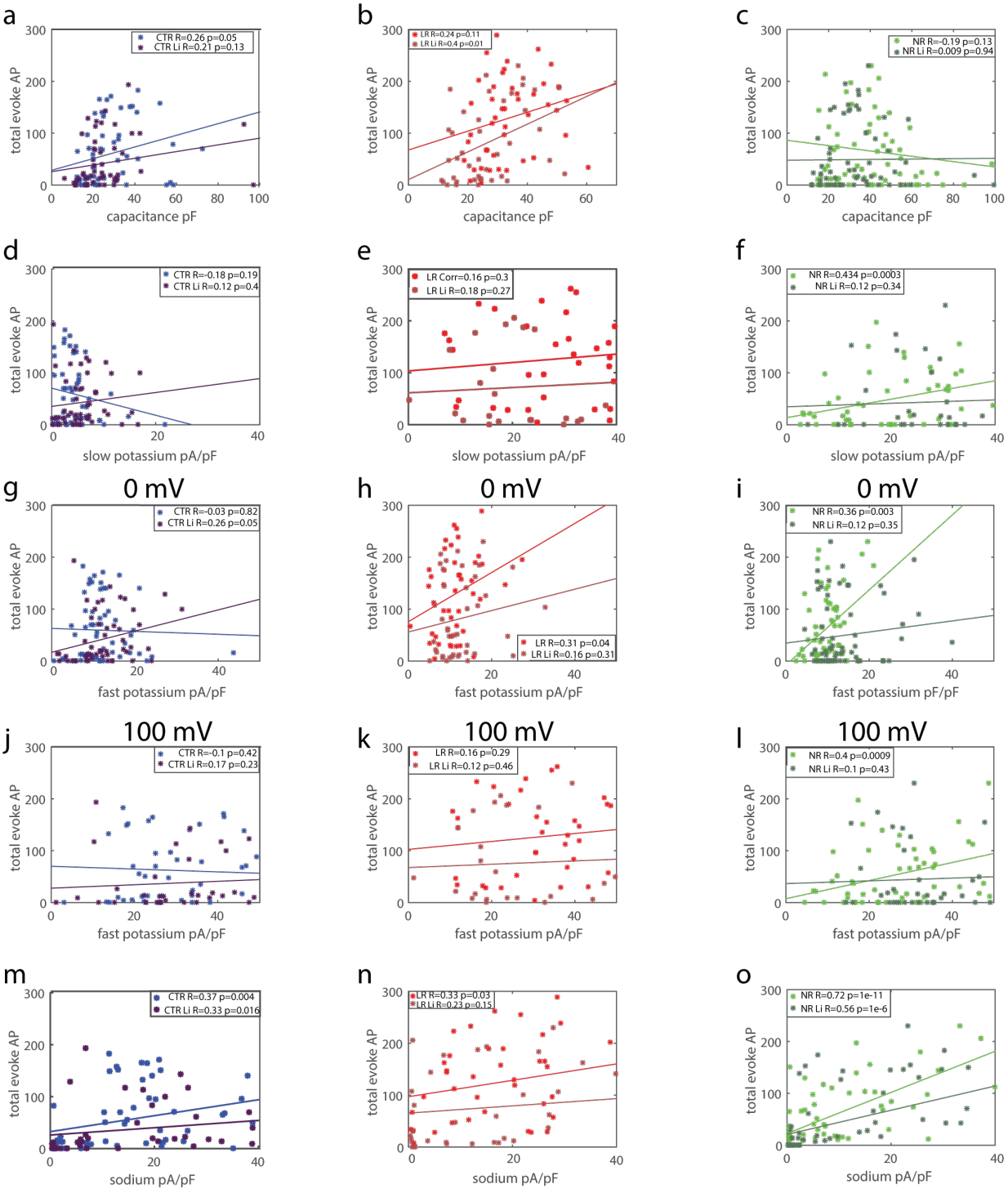

Supplementary Figure 1. Neuronal markers and potassium channels expression. a. Example images of immunostaining for 4′,6-diamidino-2-phenylindole (DAPI, blue, marks the nucleus), ELAV-like RNA

binding protein 2 **(**ELAVL2, red, specific marker of CA3 pyramidal neurons) and microtubule associated protein 2 (MAP2, green, enriched in neurites). b. Example images of immunostaining for GABA-expressing neurons in control neurons, LR and NR cultures. c. Percentage of ELAVL2-expressing neurons is approximately 60% in all 3 groups, indicating that our differentiation protocol is efficient. d. No significant change between the 3 groups in the percentage of GABA-positive neurons (ranging 10-13%).

Supplementary Figure 2. Development over time of spike shape features. a. Development from t1 to t2 of a. the fast AHP, b. spike height, c. spike width, d. threshold for evoking an action potential and e. input conductance in DG and CA3 neurons for the 3 groups: control, BD LR, and BD NR.

Supplementary Figure 3. Each dot in this figure represents one cell. The different human subjects are marked with a different shape of the dot. **a.** Comparison of excitability between DG and CA3. CA3 neurons produce more evoked potentials in the control and LR groups. In the NR group there is a similar number of evoked potentials between DG and CA3 neurons. b. Excitability at t1 (2.5 weeks). There is a significant increase in excitability in the NR and LR groups in DG neurons compared to controls, but no change in CA3 neurons between the 3 groups. This indicates that the differences between BD and control in the DG neurons appear before the differences in the CA3 neurons c. Excitability comparison between DG and CA3 neurons at t1=2.5 weeks. CA3 control neurons produce more evoked potentials than DG neurons. d. Comparison of spontaneous activity rate between DG and CA3 neurons at t2=30 days reveals similar spontaneous activity rate between DG and CA3 neurons in all 3 groups. e. No changes are observed in the spontaneous spike amplitude between the 3 groups in both DG and CA3 neurons. f. Development over the time period between t1 and t2 of neuronal excitability (total evoked action potentials) of DG and CA3 neurons of the 3 groups: control, LR and NR. Asterisks represent statistical significance by the following code: * p value<0.05, **p value<0.01, ****p<0.0001. Error bars represent standard error.

Supplementary Figure 4. Each dot in this figure represents one cell. The different human subjects are marked with a different shape of the dot. a. Comparison DG and CA3 capacitance at t2=30 days. In all groups CA3 neurons are larger than DG neurons, but statistical significance is observed in the LR and NR groups. b. Already at t1=2.5 weeks, larger cell size is observed in the BD groups in both CA3 and DG neurons, but the NR group is always the largest. C. At t1=2.5 weeks, CA3 neurons are larger than DG neurons in all 3 groups, with a significant increase in control and NR neurons. d. The capacitance to soma area ratio does not change between control, LR and NR neurons, indicating that the increase is both in the soma size and in the neurites. e. At t2=30 days, comparison of DG and CA3 fast AHP shows a significant increase in LR CA3 fast AHP compared to LR DG neurons. f. At t1=2.5 weeks, no significant change in the fast AHP is observed between the groups. g. Spike amplitude does not change between DG and CA3 neurons in all 3 groups at t2=30 days. h. The spike height at t1=2.5 weeks is larger for the DG LR group compared with DG control or DG NR. There is no change in the CA3 neurons between the 3 groups, since the maturation in CA3 neuron is delayed. i. The spike height at t1=2.5 weeks is smaller in control and LR Ca3 compared to control and LR DG neurons, further indicating slower maturation of CA3 neurons compared to DG neurons. Asterisks represent statistical significance by the following code: * p value<0.05, **p value<0.01, ***p<0.001, ****p<0.0001. Error bars represent standard error.

Supplementary Figure 5. Spike shape parameters. In this figure, each dot in the graph represents a single patched neuron. Each patient is denoted with a different shape of the dot. a. Spike width (at t2=30 days) does not significantly change between DG and CA3 neurons in any of the 3 groups. b. Spike width is narrower at t1=2.5 weeks in LR DG neurons compared to NR DG neurons. c. At t1=2.5 weeks, spike width is narrower in DG neurons compared to CA3 neurons, further indicating that DG neurons mature

faster than CA3 neurons. d. At t2=30 days, the threshold for evoking an action potential is more depolarized in the control group. e. In DG neurons at t1=2.5 week, the threshold for evoking an action potential is more depolarized in the NR neurons than in control and LR neurons. f. At t1=2.5 weeks, the threshold for evoking an action potential is more depolarized in the control (significant) and LR (significant) CA3 neurons compared to DG neurons, but in NR neurons; CA3 neurons have a less depolarized threshold for evoking an action potential. g. No significant changes in the input conductance of CA3 vs. DG neurons in all 3 groups at t2=30 days. h. No significant changes in the input conductance of CA3 vs. DG neurons in all 3 groups at t1=2.5 weeks. i. The input conductance is significantly increased in CA3 LR neurons compared to DG neurons at t1=2.5 weeks. Asterisks represent statistical significance by the following code: * p value<0.05, **p value<0.01, ***p<0.001, ****p<0.0001. Error bars represent standard error.

Supplementary Figure 6. Fpkm values of RNA sequencing from DG neurons derived from our previous cohort (Mertens et al., 2015). Similar to CA3 neurons derived from the current cohort, LR neurons have an overexpression of Kcnc2 and Kcnc3 potassium channels whereas NR neurons have a decreased expression of Kcnc3 expression.

Supplementary Figure 7. a. The fast potassium currents are increased in BD LR and BD NR CA3 neurons compared to controls. b. The fast potassium currents are similar between the control, B LR and BD NR DG neurons compared to controls. c. Sodium currents in CA3 NR neurons display a slower kinetics of closing of the channels. d. Sodium currents in CA3 NR neurons display a slower kinetics of opening of the channels e. The fast potassium currents in CA3 neurons at t1=2.5 weeks are increased in LR and even more in NR neurons. f. In DG neurons, the fast potassium currents at t1=2.5 weeks are increased in the LR neurons. g. Normalized sodium currents at t1=2.5 weeks are increased in CA3 NR neurons compared to the other groups. h. The normalized sodium currents at t1=2.5 weeks are decreased in the NR group in DG neurons. i. Further comparison of the normalized sodium currents in CA3 neurons reveals a drastic reduction of sodium currents in NR neurons at t2=30 days. j. In DG neurons at t2=30 days there is also a reduction in the normalized sodium currents, although less drastic than in the CA3 neurons. k. Calculating the sodium currents at t1=2.5 weeks in CA3 neurons reveals that there is a big fluctuation in these currents, and at t1 NR sodium currents are increased, just to later on be severely decreased. l. The sodium currents at t1=2.5 weeks in DG neurons are reduced in the NR group**.** m. The slow potassium currents are increased at t2=30 days in CA3 LR and NR neurons compared to controls n. Similar slow potassium currents are observed between the 3 groups in DG neurons at t2=30 days. o. At t1=2.5 weeks the slow potassium currents are increased in CA3 LR and NR neurons compared to control neurons. p. At t1=2.5 weeks the slow potassium currents are increased in DG LR neurons compared to control and NR neurons.

Supplementary Figure 8. qPCR of KCNMA1, KCNMB1. a. No significant change in expression of KCNMA1 gene between the 3 groups. b. No significant change in expression of KCNMB1 gene in the 3 groups.

Supplementary Figure 9. An example recording in voltage clamp mode demonstrating that, due to fluctuations in the currents, the potassium current should be calculated manually at the low (-20 mV – 20 mV) depolarization steps.

Supplementary Figure 10. Measurements after chronic lithium treatment in CA3 neurons at t2. a. The input conductance does not significantly change with lithium treatment in any of the 3 groups. b. The sodium opening kinetics (each dot representing a patched neuron) becomes faster after chronic lithium

treatment in control and NR neurons. c. Same graph as in b, but here each dot represents an average over each of the lines' (patients') recordings.

Supplementary Figure 11. BD neurons and NPCs are larger than controls. a. The capacitance of CA3 BD LR neurons is larger than the controls' capacitance, and CA3 NR neurons are even larger (around 70% increase compared to controls). [Remark: In our previous report, at around 25 days, BD DG neurons were larger than controls as well (Stern et al., 2018)] b. Development from t1=2.5 weeks to t2=30 days. c. Imaging of the soma of CA3 neurons further supports the capacitance changes: soma is larger for CA3 LR neurons and even more for CA3 NR neurons. d. The ratio of capacitance to soma size is not changed between the groups - control, BD LR and BD NR - and this indicates that there are similar larger neurites in LR BD and even more in NR BD compared to controls. e. Example of a control soma. f. Example of a BD LR soma. g. Example of a BD NR soma. h. Imaging of a total of n=30 neurons from each patient of neural progenitor cells (NPCs) further shows that there is a change in cell size as early as the NPC stage (each dot in the graph represents the average of one human subject). i. The initial neurites at the NPC stage are larger in BD NR neurons. j. A representative image of control NPCs. k. A representative image of BD LR NPCs. l. A representative image of BD NR NPCs. Asterisks represent statistical significance by the following code: * p value<0.05, **p value<0.01, ***p<0.001, ****p<0.0001. Error bars represent standard error.

Supplementary Figure 12. Correlations of CA3 excitability with currents at t2=30 days. a-c. Control and LR excitability correlates significantly with cell capacitance, but this correlation is completely lost in NR neurons. d-f. Control and LR neurons weakly correlate with the amplitude of the slow potassium currents at 10 mV, but a significant correlation is observed in NR neurons (which diminishes with lithium treatment). g-i. A strong correlation is observed between excitability and the amplitude of the fast potassium currents at 0 mV in LR and NR neurons. This correlation weakens with lithium treatment. Control neurons' excitability does not correlate with the amplitude of the fast potassium currents at 0 mV, but this correlation is seen with lithium treatment. j-l. Control and LR excitability does not correlate with the amplitude of the fast potassium current at 100 mV. However, NR excitability does correlate with the amplitude of the fast potassium current at 100 mV. This correlation diminishes after lithium treatment. m-o. All the groups correlate with sodium currents (at -20 mV). This correlation is much stronger in NR neurons compared to control and LR neurons, and so is the incline of the graph. This correlation weakens a bit with lithium treatment but remains very significant.

References

Abe, C., Ekman, C.J., Sellgren, C., Petrovic, P., Ingvar, M., and Landen, M. (2015). Manic episodes are related to changes in frontal cortex: a longitudinal neuroimaging study of bipolar disorder 1. Brain : a journal of neurology *138*, 3440-3448.

Altshuler, L.L., Bartzokis, G., Grieder, T., Curran, J., and Mintz, J. (1998). Amygdala enlargement in bipolar disorder and hippocampal reduction in schizophrenia: an MRI study demonstrating neuroanatomic specificity. Archives of general psychiatry *55*, 663-664.

Baum, A.E., Akula, N., Cabanero, M., Cardona, I., Corona, W., Klemens, B., Schulze, T.G., Cichon, S., Rietschel, M., Nothen, M.M*., et al.* (2008). A genome-wide association study implicates diacylglycerol kinase eta (DGKH) and several other genes in the etiology of bipolar disorder. Molecular psychiatry *13*, 197-207.

Bekkers, J.M., and Delaney, A.J. (2001). Modulation of excitability by alpha-dendrotoxin-sensitive potassium channels in neocortical pyramidal neurons. J Neurosci *21*, 6553-6560.

Beyer, J.L., Kuchibhatla, M., Payne, M.E., Moo-Young, M., Cassidy, F., Macfall, J., and Krishnan, K.R. (2004). Hippocampal volume measurement in older adults with bipolar disorder. Am J Geriatr Psychiatry *12*, 613-620.

Bezchlibnyk, Y.B., Wang, J.F., McQueen, G.M., and Young, L.T. (2001). Gene expression differences in bipolar disorder revealed by cDNA array analysis of post-mortem frontal cortex. Journal of neurochemistry *79*, 826-834.

Blumberg, H.P., Kaufman, J., Martin, A., Whiteman, R., Zhang, J.H., Gore, J.C., Charney, D.S., Krystal, J.H., and Peterson, B.S. (2003). Amygdala and hippocampal volumes in adolescents and adults with bipolar disorder. Archives of general psychiatry *60*, 1201-1208.

Brambilla, P., Harenski, K., Nicoletti, M., Sassi, R.B., Mallinger, A.G., Frank, E., Kupfer, D.J., Keshavan, M.S., and Soares, J.C. (2003). MRI investigation of temporal lobe structures in bipolar patients. Journal of psychiatric research *37*, 287-295.

Cao, B., Bauer, I.E., Sharma, A.N., Mwangi, B., Frazier, T., Lavagnino, L., Zunta-Soares, G.B., Walss-Bass, C., Glahn, D.C., Kapczinski, F*., et al.* (2016). Reduced hippocampus volume and memory performance in bipolar disorder patients carrying the BDNF val66met met allele. Journal of affective disorders *198*, 198-205.

Cao, B., Passos, I.C., Mwangi, B., Amaral-Silva, H., Tannous, J., Wu, M.J., Zunta-Soares, G.B., and Soares, J.C. (2017). Hippocampal subfield volumes in mood disorders. Molecular psychiatry *22*, 1352-1358.

Fatemi, S.H., Earle, J.A., and McMenomy, T. (2000). Reduction in Reelin immunoreactivity in hippocampus of subjects with schizophrenia, bipolar disorder and major depression. Molecular psychiatry *5*, 654-663, 571.

Ferreira, M.A., O'Donovan, M.C., Meng, Y.A., Jones, I.R., Ruderfer, D.M., Jones, L., Fan, J., Kirov, G., Perlis, R.H., Green, E.K*., et al.* (2008). Collaborative genome-wide association analysis supports a role for ANK3 and CACNA1C in bipolar disorder. Nature genetics *40*, 1056-1058.

Forstner, A.J., Hecker, J., Hofmann, A., Maaser, A., Reinbold, C.S., Muhleisen, T.W., Leber, M., Strohmaier, J., Degenhardt, F., Treutlein, J.*, et al.* (2017). Identification of shared risk loci and pathways for bipolar disorder and schizophrenia. PloS one *12*, e0171595.
Gawryluk, J.W., Wang, J.F., Andreazza, A.C., Shao, L., and Young, L.T. (2011). Decreased levels of glutathione, the major brain antioxidant, in post-mortem prefrontal cortex from patients with psychiatric disorders. The international journal of neuropsychopharmacology *14*, 123-130.
Gershon, E.S., Alliey-Rodriguez, N., and Liu, C. (2011). After GWAS: searching for genetic risk for schizophrenia and bipolar disorder. The American journal of psychiatry *168*, 253-256.
Gitlin, M. (2016). Lithium side effects and toxicity: prevalence and management strategies. International journal of bipolar disorders *4*, 27.
Grande, I., Berk, M., Birmaher, B., and Vieta, E. (2016). Bipolar disorder. Lancet *387*, 1561-1572.
Green, E.K., Grozeva, D., Jones, I., Jones, L., Kirov, G., Caesar, S., Gordon-Smith, K., Fraser, C., Forty, L., Russell, E.*, et al.* (2010). The bipolar disorder risk allele at CACNA1C also confers risk of recurrent major depression and of schizophrenia. Molecular psychiatry *15*, 1016-1022.
Hajek, T., Kopecek, M., Hoschl, C., and Alda, M. (2012). Smaller hippocampal volumes in patients with bipolar disorder are masked by exposure to lithium: a meta-analysis. J Psychiatry Neurosci *37*, 333-343.
Hibar, D.P., Westlye, L.T., Doan, N.T., Jahanshad, N., Cheung, J.W., Ching, C.R.K., Versace, A., Bilderbeck, A.C., Uhlmann, A., Mwangi, B.*, et al.* (2018). Cortical abnormalities in bipolar disorder: an MRI analysis of 6503 individuals from the ENIGMA Bipolar Disorder Working Group. Molecular psychiatry *23*, 932-942.
Huang, J., Perlis, R.H., Lee, P.H., Rush, A.J., Fava, M., Sachs, G.S., Lieberman, J., Hamilton, S.P., Sullivan, P., Sklar, P.*, et al.* (2010). Cross-disorder genomewide analysis of schizophrenia, bipolar disorder, and depression. The American journal of psychiatry *167*, 1254-1263.
Jamison, K.R. (2000). Suicide and bipolar disorder. The Journal of clinical psychiatry *61 Suppl 9*, 47-51.
Javadapour, A., Malhi, G.S., Ivanovski, B., Chen, X., Wen, W., and Sachdev, P. (2010). Hippocampal volumes in adults with bipolar disorder. J Neuropsychiatry Clin Neurosci *22*, 55-62.
Kaczmarek, L.K., and Zhang, Y. (2017). Kv3 Channels: Enablers of Rapid Firing, Neurotransmitter Release, and Neuronal Endurance. Physiol Rev *97*, 1431-1468.
Kim, K.H., Liu, J., Sells Galvin, R.J., Dage, J.L., Egeland, J.A., Smith, R.C., Merchant, K.M., and Paul, S.M. (2015). Transcriptomic Analysis of Induced Pluripotent Stem Cells Derived from Patients with Bipolar Disorder from an Old Order Amish Pedigree. PloS one *10*, e0142693.
Lawrence, N.S., Williams, A.M., Surguladze, S., Giampietro, V., Brammer, M.J., Andrew, C., Frangou, S., Ecker, C., and Phillips, M.L. (2004). Subcortical and ventral prefrontal cortical neural responses to facial expressions distinguish patients with bipolar disorder and major depression. Biological psychiatry *55*, 578-587.
Madison, J.M., Zhou, F., Nigam, A., Hussain, A., Barker, D.D., Nehme, R., van der Ven, K., Hsu, J., Wolf, P., Fleishman, M.*, et al.* (2015). Characterization of bipolar disorder patient-specific induced pluripotent stem cells from a family reveals neurodevelopmental and mRNA expression abnormalities. Molecular psychiatry *20*, 703-717.
Marchetto, M.C., Muotri, A.R., Mu, Y., Smith, A.M., Cezar, G.G., and Gage, F.H. (2008). Non-cell-autonomous effect of human SOD1 G37R astrocytes on motor neurons derived from human embryonic stem cells. Cell stem cell *3*, 649-657.
Martina, M., Schultz, J.H., Ehmke, H., Monyer, H., and Jonas, P. (1998). Functional and molecular differences between voltage-gated K+ channels of fast-spiking interneurons and pyramidal neurons of rat hippocampus. J Neurosci *18*, 8111-8125.
Merikangas, K.R., Akiskal, H.S., Angst, J., Greenberg, P.E., Hirschfeld, R.M., Petukhova, M., and Kessler, R.C. (2007). Lifetime and 12-month prevalence of bipolar spectrum disorder in the National Comorbidity Survey replication. Archives of general psychiatry *64*, 543-552.

Mertens, J., Wang, Q.W., Kim, Y., Yu, D.X., Pham, S., Yang, B., Zheng, Y., Diffenderfer, K.E., Zhang, J., Soltani, S.*, et al.* (2015). Differential responses to lithium in hyperexcitable neurons from patients with bipolar disorder. Nature *527*, 95-99.
Muhleisen, T.W., Leber, M., Schulze, T.G., Strohmaier, J., Degenhardt, F., Treutlein, J., Mattheisen, M., Forstner, A.J., Schumacher, J., Breuer, R.*, et al.* (2014). Genome-wide association study reveals two new risk loci for bipolar disorder. Nature communications *5*, 3339.
Neves-Pereira, M., Mundo, E., Muglia, P., King, N., Macciardi, F., and Kennedy, J.L. (2002). The brain-derived neurotrophic factor gene confers susceptibility to bipolar disorder: evidence from a family-based association study. American journal of human genetics *71*, 651-655.
Psychiatric, G.C.B.D.W.G. (2011). Large-scale genome-wide association analysis of bipolar disorder identifies a new susceptibility locus near ODZ4. Nature genetics *43*, 977-983.
Rajkowska, G., Halaris, A., and Selemon, L.D. (2001). Reductions in neuronal and glial density characterize the dorsolateral prefrontal cortex in bipolar disorder. Biological psychiatry *49*, 741-752.
Rudy, B. (1988). Diversity and ubiquity of K channels. Neuroscience *25*, 729-749.
Sarkar, A., Mei, A., Paquola, A.C.M., Stern, S., Bardy, C., Klug, J.R., Kim, S., Neshat, N., Kim, H.J., Ku, M.*, et al.* (2018). Efficient Generation of CA3 Neurons from Human Pluripotent Stem Cells Enables Modeling of Hippocampal Connectivity In Vitro. Cell stem cell *22*, 684-697 e689.
Senzai, Y., and Buzsaki, G. (2017). Physiological Properties and Behavioral Correlates of Hippocampal Granule Cells and Mossy Cells. Neuron *93*, 691-704 e695.
Stelzhammer, V., Alsaif, M., Chan, M.K., Rahmoune, H., Steeb, H., Guest, P.C., and Bahn, S. (2015). Distinct proteomic profiles in post-mortem pituitary glands from bipolar disorder and major depressive disorder patients. Journal of psychiatric research *60*, 40-48.
Stern, S., Santos, R., Marchetto, M.C., Mendes, A.P.D., Rouleau, G.A., Biesmans, S., Wang, Q.W., Yao, J., Charnay, P., Bang, A.G.*, et al.* (2018). Neurons derived from patients with bipolar disorder divide into intrinsically different sub-populations of neurons, predicting the patients' responsiveness to lithium. Molecular psychiatry *23*, 1453-1465.
Stern, S., Segal, M., and Moses, E. (2015). Involvement of Potassium and Cation Channels in Hippocampal Abnormalities of Embryonic Ts65Dn and Tc1 Trisomic Mice. EBioMedicine *2*, 1048-1062.
Strakowski, S.M., DelBello, M.P., Sax, K.W., Zimmerman, M.E., Shear, P.K., Hawkins, J.M., and Larson, E.R. (1999). Brain magnetic resonance imaging of structural abnormalities in bipolar disorder. Archives of general psychiatry *56*, 254-260.
Strakowski, S.M., DelBello, M.P., Zimmerman, M.E., Getz, G.E., Mills, N.P., Ret, J., Shear, P., and Adler, C.M. (2002). Ventricular and periventricular structural volumes in first- versus multiple-episode bipolar disorder. The American journal of psychiatry *159*, 1841-1847.
Tobe, B.T.D., Crain, A.M., Winquist, A.M., Calabrese, B., Makihara, H., Zhao, W.N., Lalonde, J., Nakamura, H., Konopaske, G., Sidor, M.*, et al.* (2017). Probing the lithium-response pathway in hiPSCs implicates the phosphoregulatory set-point for a cytoskeletal modulator in bipolar pathogenesis. Proceedings of the National Academy of Sciences of the United States of America *114*, E4462-E4471.
Van Meter, A.R., Moreira, A.L., and Youngstrom, E.A. (2011). Meta-analysis of epidemiologic studies of pediatric bipolar disorder. The Journal of clinical psychiatry *72*, 1250-1256.
Videbech, P., and Ravnkilde, B. (2004). Hippocampal volume and depression: a meta-analysis of MRI studies. The American journal of psychiatry *161*, 1957-1966.
Yu, D.X., Di Giorgio, F.P., Yao, J., Marchetto, M.C., Brennand, K., Wright, R., Mei, A., McHenry, L., Lisuk, D., Grasmick, J.M.*, et al.* (2014). Modeling hippocampal neurogenesis using human pluripotent stem cells. Stem cell reports *2*, 295-310.
Zung, S., Souza-Duran, F.L., Soeiro-de-Souza, M.G., Uchida, R., Bottino, C.M., Busatto, G.F., and Vallada, H. (2016). The influence of lithium on hippocampal volume in elderly bipolar patients: a study using voxel-based morphometry. Transl Psychiatry *6*, e846.